Subcellular localization requirements and specificities for plant immune receptor Toll-interleukin-1 receptor (TIR) signaling

M. Bernoux, Jian Chen, Xiaoxiao Zhang, Kim Newell, Jian Hu, Laurent Deslandes, Peter Dodds

Title: Subcellular localization requirements and specificities for plant immune receptor Toll-interleukin-1 receptor (TIR) signaling

Maud Bernoux[1]*, Jian Chen[2], Xiaoxiao Zhang[3], Kim Newell[2], Jian Hu[4], Laurent Deslandes[1], Peter Dodds[2]

1-Laboratoire des Interactions Plantes-Microbes-Environnement (LIPME), UMR 2594/441 CNRS, INRAE, 31326, Castanet-Tolosan, France.
2-Agriculture and Food, Commonwealth Scientific and Industrial Research Organization, Canberra, ACT2601, Australia
3-Research School of Biology, Australian National University, Canberra, ACT 2601, Australia
4-Department of Biochemistry and Molecular Biology, College of Biological Sciences, China Agricultural University, Beijing 100094, P.R. China.

Running title: TIR signaling subcellular localization requirement

Keywords: NLR cell biology, TIR signaling, EDS1, *Arabidopsis thaliana*, *Nicotiana benthamiana*

***Corresponding author details:**
maud.bernoux@inrae.fr
Laboratoire des Interactions Plantes-Microbes-Environnement (LIPME), UMR 2594/441 CNRS, INRAE, 31326, Castanet-Tolosan, France.

SUMMARY

Recent work shed light on how plant intracellular immune receptors of the nucleotide-binding leucine-rich repeat (NLR) family are activated upon pathogen effector recognition to trigger immune responses. Activation of Toll-interleukin-1 receptor (TIR) domain-containing NLRs (TNLs) induces receptor oligomerization and close proximity of the TIR domain, which is required for TIR enzymatic activity. TIR-catalysed small signaling molecules bind to EDS1 family heterodimers and subsequently activate downstream helper NLRs, which function as Ca^{2+} permeable channel to activate immune responses eventually leading to cell death. Subcellular localisation requirements of TNLs and signaling partners are not well understood, although they are required to fully understand the mechanisms underlying NLR early signaling. TNLs show diverse subcellular localization while EDS1 shows nucleocytosolic localization. Here, we studied the impact of TIR and EDS1 mislocalization on the signaling activation of different TNLs. In *N. benthamiana*, our results suggest that close proximity of TIR domains isolated from flax L6 and Arabidopsis RPS4 and SNC1 TNLs drives signaling activation from different cell compartments. Nevertheless, both Golgi-membrane anchored L6 and nucleocytosolic RPS4 have the same requirements for EDS1 subcellular localization in *Arabidopsis thaliana*. By using mislocalized variants of EDS1, we found that autoimmune L6 and RPS4 TIR domain can induce seedling cell death when EDS1 is present in the cytosol. However, when EDS1 is restricted to the nucleus, both induce a stunting phenotype but no cell death.

Our data point out the importance of thoroughly investigating the dynamics of TNLs and signaling partners subcellular localization to fully understand TNL signaling.

INTRODUCTION

Plant immunity relies on a combination of cell-surface and intracellular receptors that perceive infection-associated molecules (Dodds and Rathjen, 2010). Cell surface receptors, also called pattern-recognition receptors (PRRs), are anchored to the cell plasma membrane to recognize extracellular signals via their ectodomain. Intracellular receptors belong to the nucleotide-binding leucine-rich repeat receptor (NLR) family, whose modular architecure is similar to animal receptors involved in innate immunity and apoptosis (Bentham et al., 2016; Duxbury et al., 2016). Most NLRs specifically sense, directly or indirectly, the presence of pathogen effectors that are secreted inside the plant cell (Zhang et al., 2017a). Although cell surface and intracellular immune receptors are structurally different and localize to different subcellular compartments, their activation induces largely overlapping immune responses (reactive oxygen species production, MAPKinase cascade

activation, ion fluxes, a massive transcriptional reprogramming, and sometimes the induction of cell death) (Lu and Tsuda, 2021). Increasing evidence suggest that PRR- and NLR-mediated signaling pathway mutually potentiate each other (Bernoux et al., 2022).

Canonical NLRs contain three modules: the C-terminal leucine-rich repeat (LRR) domain often acts as a sensor that allows specific pathogen effector recognition. The central nucleotide binding (NB) domain controls the switch between inactive (OFF) and active (ON) states with a massive conformational change upon activation (Bernoux et al., 2016; Wang et al., 2019b). The N-terminal domain often acts as a signaling domain. In flowering plants, this region commonly contains a coiled-coil (CC) or Toll-interleukin-1 receptor (TIR) domain. The TIR domain is involved in immune signaling pathways across phyla (Ve et al., 2015; Essuman et al., 2022). Upon effector recognition, several NLRs have been shown to associate into oligomeric complexes termed resistosomes, which is required to further activate downstream signaling (Wang et al., 2019a; Ma et al., 2020; Martin et al., 2020). The 3D structure of the Arabidopsis ZAR1 and wheat Sr35 CC-containing NLRs (CNLs) showed that ZAR1 and Sr35 form a pentamer upon activation and the N-terminal CC domain complex forms a funnel-like structure similar to pore-forming proteins (Wang et al., 2019a; Förderer et al., 2022). Further studies revealed that activated ZAR1 targets the plasma membrane and functions as Ca^{2+} permeable channels via its CC domain, to rapidly activate immune responses (Bi et al., 2021). Signaling of TIR-containing NLRs (TNLs) is more complex. Structural analyses of *N. benthamiana* TNLs ROQ1 and Arabidopsis RPP1 revealed a tetrameric resistosome upon effector recognition. TNL oligomerization lead to the induced proximity of the N-terminal TIR domains, which create access to the TIR NADase catalytic site (Gerdts et al., 2015; Horsefield et al., 2019; Wan et al., 2019; Ma et al., 2020; Martin et al., 2020). TIR complex assembly can also result in a helix-like structure. Depending on the TIR self-association interface and protein complex stoichiometry (tetramer or helix), TIR domains display different enzymatic activity by using different substrates (NAD(P) and DNA/RNA, respectively), to release small signaling molecules (Horsefield et al., 2019; Wan et al., 2019; Huang et al., 2022; Jia et al., 2022; Yu et al., 2022). All sensor TNLs studied so far require the nucleocytoplasmic lipase-like EDS1 (ENHANCED DISEASE SUSCEPTIBILITY 1) to activate immune responses (Wiermer et al., 2005; Lapin et al., 2020). EDS1 forms mutually exclusive heterodimers with two other members of the EDS1 family, SAG101 (SENESCENCE-ASSOCIATED GENE 101) or PAD4 (PHYTOALEXIN DEFICIENT 4) (Lapin et al., 2020). Upon TNL activation, EDS1/PAD4 or EDS1/SAG101 bind distinct TIR-catalysed NAD(P)-derived small molecules and subsequently associate with the downstream helper CC_R-containing NLRs (RNLs), ADR1 and NRG1, respectively (Huang et al., 2022; Jia et al., 2022). Like ZAR1, autoactivated NRG1 also seems to oligomerize and form Ca^{2+} permeable channels at the

plasma membrane (Jacob et al., 2021), suggesting the ultimate output of TNLs signaling is CNL-induced Ca^{2+} influx to activate immune responses (Jacob et al., 2021).

Nevertheless, it is unclear where in the cell does the activation of TNLs and the first steps of signaling occurs, and whether this is conserved across NLRs. TNLs are distributed in a range of subcellular locations and NLR mislocalization often affects their function (Takemoto et al., 2012). Nucleocytosplasmic transport can also play an important role for regulating immune complex formation and signaling activation upon NLR activation, including for EDS1 function (Lüdke et al., 2022). Arabidopsis SNC1 and RPS4 TNLs both display a nucleocytoplasmic localization while flax L6 is anchored to the Golgi membrane (Wirthmueller et al., 2007; Cheng et al., 2009; Takemoto et al., 2012). Flax L6 confers resistance to the fungal pathogen *Melampsora lini* (flax rust) producing the AvrL567 effector (Dodds et al., 2006). Releasing L6 from the Golgi membrane impacts L6-mediated resistance to flax rust (Takemoto et al., 2012). RPS4 functions in concert with another TNL, RRS1, to activate disease resistance upon recognition of AvrRps4 and PopP2 effectors from *Pseudomonas syringae* and *Ralstonia solanacearum* bacterial pathogens, respectively. RRS1 acts as a sensor to recognize the presence of the effectors via its integrated WRKY domain, while RPS4 translates the signal via its TIR domain (Williams et al., 2014; Le Roux et al., 2015; Sarris et al., 2015). Nuclear pools of SNC1 and RPS4 were shown to be required for their signaling function (Wirthmueller et al., 2007; Cheng et al., 2009; Xu et al., 2014). However, both RPS4 and SNC1 function depends on RNLs ADR1 and NRG1, which are thought to activate immune responses at the plasma membrane (Dong et al., 2016; Wu et al., 2019; Saile et al., 2020; Saile et al., 2021). Earlier studies showed that EDS1 physically interacts with some NLRs, including RPS4 and SNC1 (Bhattacharjee et al., 2011; Heidrich et al., 2011; Kim et al., 2012; Huh et al., 2017; Zhang et al., 2019), and that a balanced cytosolic and nuclear shuttle of EDS1 is important for Arabidopsis basal and TNL-mediated immunity (García et al., 2010). However, a bifurcation between nuclear and cytosolic EDS1 activities was also previously suggested with the nuclear fraction being involved in gene reprogramming while the cytosolic pool is involved in cell death activation (Heidrich et al., 2011; Lapin et al., 2019). Hence, it is intriguing to know how and in which subcellular compartment do TNLs that are not nucleo-cytosolic, such as L6, function with EDS1 to activate downstream signaling defense pathway.

In this study, we investigated the subcellular localization requirement of three TIR domains isolated from different TNLs, as well as EDS1, for the activation of TIR signaling. We first studied the signaling function of mislocalized TIR domains isolated from flax L6, and Arabidopsis RPS4 and SNC1 NLR, as these TIR domains function as signaling unit on their own. They can induce pathogen-independent defence signaling when overexpressed *in planta*, including the heterologous model plant *Nicotiana benthamiana* (Swiderski et al., 2009; Bernoux et al., 2011; Williams et al., 2014; Zhang et

al., 2017b) and thus can be used as a tool to study TNL early signaling events. We also determined the impact of EDS1 mislocalization on TIR signaling in transgenic Arabidopsis lines co-expressing inducible autoimmune flax L6 variant or RPS4TIR domain with mislocalized EDS1 variants.

RESULTS

Membrane attachment of flax L6TIR domain is required for its signaling activity

The flax TNLs L6 and M are targeted to the Golgi and vacuole membrane, respectively, due to the presence of hydrophobic residues in their N-terminal sequence. In contrast, the flax P2 protein lacks such N-terminal extension and does not target cellular membranes (Takemoto et al., 2012). Domain swaps between the N-terminal sequence of L6, M and P2 revealed that membrane attachment contributes to L6 resistance function against flax rust *Melampsora lini* containing corresponding effector AvrL567 in flax (Takemoto et al., 2012).

To decipher whether membrane attachment is required for L6 signaling function, we studied the subcellular localization requirements of isolated L6 TIR by using recombinants containing M or P2 N-terminal sequences, based on constructs used in Takemoto et al. (2012), fused to the yellow fluorescent protein (YFP). After Agrobacterium-mediated transient expression in flax leaves, confocal analysis showed that L6TIR-YFP displays a punctate pattern of fluorescence similar to that of L6 full-length protein, typical of Golgi membrane labeling (Figure 1A) (Takemoto et al., 2012). As previously reported, L6TIR-YFP signaling activity triggered a cell death/chlorosis phenotype upon transient overexpression in flax, a proxy for NLR-mediated immune response activation (c) (Bernoux et al., 2011). In contrast, expression of P2/L6TIR-YFP variant did not show any Golgi body labelling but instead showed fluorescence in both nuclear and cytosolic compartments and did not induce cell death (Figure 1B, 1F), although it also showed lower protein accumulation (Figure 1I)). Interestingly, mislocalization of L6TIR to a different membrane (tonoplast) (M/L6TIR-YFP) does not affect L6TIR signaling activity (Figure 1C, 1G), whereas a mutation in M signal anchor (M*) that releases most of M*/L6TIR from the vacuole membrane to the nucleocytosol (Takemoto et al., 2012) displays much weaker signaling activity compared to M/L6TIR (Figure 1D, 1H). Both M/L6TIR and M*/L6TIR recombinant proteins accumulated at a similar level (Figure 1I), supporting that membrane attachment is important for L6TIR signaling activity. One possible explanation to explain these results is that concentration of the L6TIR domain at the membrane induces its self-association, which is required to activate signaling (Bernoux et al., 2011; Horsefield et al., 2019; Duxbury et al., 2020). Hence, releasing L6TIR to the nucleocytosol would reduce L6TIR self-association and prevent signaling. This hypothesis is supported by recent structural evidence that activated TNLs form oligomeric complexes that bring the N-terminal TIR domains into close proximity to activate its

NADase enzymatic activity (Wang et al., 2019a; Ma et al., 2020; Martin et al., 2020).

Close proximity of L6TIR domain drives signaling activation from the cytosolic compartment in flax and *Nicotiana benthamiana*

Given that the membrane localisation of L6TIR is likely a requirement for oligomerisation rather than a locational restraint on signaling, we further investigated the subcellular requirement for L6TIR signaling function, by using the nucleocytosolic P2/L6TIR recombinant as a tool. When expressed on its own, P2/L6TIR cannot activate signaling (Figure 1F). To test whether close proximity of P2/L6TIR can activate TIR signaling, we fused P2/L6TIR to the flax rust effector AvrM, which was previously reported to form a stable dimer *in planta* (Catanzariti et al., 2010; Ve et al., 2013). When overexpressed in flax leaves of the Hoshangabad flax genotype, AvrM does not trigger any cell death symptoms (Catanzariti et al., 2006). However, overexpression of P2/L6TIR-AvrM fusion induced a similar response to L6TIR-YFP or L6TIR-AvrM (Figure S1A), suggesting that dimerization of AvrM can promote P2/L6TIR signaling. To examine from which compartment (cytosol or nucleus) can L6TIR activate signaling, we generated a series of constructs consisting of signaling active (P2L6TIR-AvrM) or inactive (P2/L6TIR) recombinants fused to YFP, with a nuclear localization signal (NLS) or a nuclear exclusion signal (NES) and corresponding mutants (nls and nes, respectively). Upon transient expression in flax leaves, all constructs from the P2/L6TIR-YFP-NLS/NES series triggered a very weak response (chlorosis) similar to the control P2/L6TIR-YFP. In contrast, all the variants of P2/L6TIR-AvrM-YFP induced a response that was similar to L6TIR-YFP positive control, except the P2/L6TIR-AvrM-YFP-NLS construct (Figure 2A). The same set of constructs trigger similar responses when expressed in the heterologous plant *Nicotiana benthamiana*, suggesting that L6 TIR has the same subcellular requirement for signaling activity in both plant species (Figure 2B). To validate this result, we performed ion leakage measurements, a quantitative indicator of cell death intensity. The amount of ion released in *N. benthamiana* leaf samples expressing inactive P2/L6TIR-YFP fusions series was similar to those expressing nuclear restricted P2/L6TIR-AvrM-YFP-NLS or those infiltrated with an empty *A. tumefaciens* strain. In contrast, leaves expressing the NES, nes or nls fusion constructs from the P2/L6TIR-AvrM-YFP series caused significantly higher ion leakage, demonstrating that P2/L6TIR-AvrM-YFP can activate cell death signaling in the cytosolic compartment but not in the nucleus (Figure 2C). Immunoblot analysis confirmed that the inactive P2/L6TIR-AvrM-YFP-NLS fusion was expressed at similar levels to the active versions in both flax and *N. benthamiana* (Figure 2D,E).

Confocal microscopy showed that the NLS fusion proteins were detected exclusively in the nucleus and the nucleolus, whereas NES fusions exhibited fluorescence in the cytoplasm and at the nuclear rim, consistent with nuclear exclusion. P2/L6TIR-YFP fusions to nls and nes inactive variants

targeted both nuclear and cytosolic compartments (Figure 2F). The P2/L6TIR-AvrM-YFP-nls and -nes fusions were mostly or fully excluded from the nucleus, respectively (Figure 2F), which is similar to the localisation of AvrM which is exclusively cytosolic (Figure S1B), likely due to its large size preventing nuclear diffusion in the absence of an NLS (Ve et al., 2013).

Finally, to check that the NLS sequence in the AvrM-YFP fusion constructs does not itself disrupt L6TIR signaling activity, we generated the same set of fusion constructs with signaling active L6TIR including its signal anchor. These constructs all induced an immune response in flax that was similar to the control L6TIR-YFP and the fusion proteins, including those with the NLS, were all still tethered to the Golgi membrane and showed similar accumulation (Figure S2). Altogether, these results show that the signaling potent P2/L6TIR-AvrM construct cannot induce cell death when restricted to the nucleus.

Close proximity of Arabidopsis RPS4 and SNC1 TIR domains drives signaling activation from both nuclear and cytosolic compartments in *N. benthamiana*

To decipher whether TIR domains isolated from other NLRs have, like L6TIR, specific subcellular requirements for their signaling activity, we performed a similar analysis with Arabidopsis RPS4TIR and SNC1TIR signaling domains. Unlike L6, RPS4 and SNC1 do not contain a membrane anchor in their N-terminus and show a nucleocytoplasmic distribution (Wirthmueller et al., 2007; Cheng et al., 2009).

Overexpression of RPS4 and SNC1 TIR fragments consisting of the structurally defined TIR domain with an additional 42 or 47 residues respectively (RPS4TIR $^{1-235}$ and SNC1TIR $^{1-226}$) induce a pathogen-independent immune response in *N. benthamiana* or *N. tabacum* (Swiderski et al., 2009; Williams et al., 2014; Zhang et al., 2017b). Interestingly, transient expression of YFP fusions of TIR-only constructs (RPS4TIR$^{1-193}$ and SNC1TIR$^{1-179}$) did not induce immune signaling in *N. benthamiana* or *N. tabacum* in contrast to the larger TIR fragments RPS4TIR$^{1-235}$ and SNC1TIR$^{1-226}$ (Figure 3A, B). Confocal microscopy and immunoblot analyses showed that all the fusion proteins were present in both the cytosol and the nucleus but not the nucleolus, and accumulated at similar levels (Figure S3, Figure 3C). Hence, like L6, the RPS4 and SNC1 TIR domains alone are not sufficient to activate a proper signaling response and require an extra peptide sequence, here in the C-terminal end of the TIR domain, possibly also to promote oligomerization.

To determine in which subcellular compartment RPS4 and SNC1 TIR domains activate signaling, we generated a series of fusion constructs consisting of the signaling inactive (RPS4$^{1-193}$ and SNC1$^{1-179}$) and signaling active (RPS4 $^{1-235}$ and SNC1 $^{1-226}$) TIRs fused to YFP, with NLS or NES signals, with or without fusion to the dimerizing AvrM. Unlike the P2/L6TIR, fusions of the inactive RPS4$^{1-193}$ and SNC1$^{1-179}$ TIR alone fragments to AvrM did not lead to any activation of cell death signaling

after transient expression in *N. benthamiana*. However, we observed that these inactive RPS4$^{1-193}$ and SNC1$^{1-179}$ TIR alone fragments with an NLS fusion induced cell death, with or without the AvrM fusion (Figure 3 D-G). In contrast, RPS4$^{1-193}$ and SNC1$^{1-179}$ constructs fused to NES, or nes and nls mutants, did not trigger an immune response with the exception of RPS4$^{1-193}$-YFP-nls. These findings were also supported by ion leakage measurements (Figure 3 H,I).

Immunoblot analysis showed that all the fusion proteins were expressed except SNC1$^{1-179}$-YFP-nls, which could not be detected. The protein constructs that triggered a cell death response, such as RPS4$^{1-193}$-NLS fusions (with and without AvrM) and RPS4$^{1-193}$-YFP-nls, also accumulated at lower level (Figure 3J,K), likely because protein samples were taken at the onset of cell death and protein degradation.

Confocal microscopy revealed that the NLS and NES peptides functioned as expected to sequester the TIR-YFP and TIR-AvrM-YFP constructs to the nuclear or cytosolic compartment, respectively (Figure S4). While the TIR-YFP fusions with the nes fusion showed nucleocytosolic labelling, TIR-AvrM-YFP-nes constructs were restricted to the cytosol, due to the cytosolic retention of AvrM (Figure S4, Figure S1B, (Ve et al., 2013)). In constrast, TIR-AvrM-YFP-nls constructs were mainly cystosolic but also showed weak labelling in the nucleus, while RPS4$^{1-193}$-YFP-nls was mainly targeted to the nucleus (Figure S4A). This could explain why this latter construct induced a similar immune response to RPS4$^{1-193}$-YFP-NLS. This phenotype was not observed with SNC1$^{1-179}$-YFP-nls as this protein construct did not express. Altogether, these results indicate that confining the RPS4 and SNC1 TIR domains to the nucleus induces signaling, possibly because the increased protein concentration in a smaller compartment may be sufficient to induce TIR oligomerisation. In contrast, a fusion to AvrM did not induce RPS4 and SNC1 TIR-only signaling, in contrast to P2/L6TIR.

The above results suggested that the RPS4 and SNC1 TIRs can signal cell death from the nucleus but were inconclusive with regards to potential cytosolic signaling. To address this question, we generated a similar YFP-NLS/NES fusion series for the larger autonomously active RPS4TIR$^{1-235}$ and SNC1TIR$^{1-226}$ proteins. Interestingly, all tested RPS4TIR$^{1-235}$ and SNC1TIR$^{1-226}$ TIR-YFP constructs fused to NLS or NES and mutated nls and nes induced a strong immune response when overexpressed in *N. benthamiana*, except for SNC1TIR $^{1-226}$ -YFP-nls (Figure 4 A-B). Immunoblot analysis revealed that the inactive SNC1TIR$^{1-226}$-YFP-nls construct did not accumulate at all, similarly to SNC1TIR$^{1-179}$-YFP-nls, for unknown reasons. This analysis also showed that NLS fusions of both RPS4TIR$^{1-235}$ and SNC1TIR$^{1-226}$ -YFP accumulate less than the other constructs, although they still induce a cell death response (Figure 4C,D). Examination of the subcellular localization of these constructs showed the expected localizations, although the RPS4TIR$^{1-235}$-YFP-NES fusions was not completely excluded from the nucleus, which still showed some weak nuclear fluorescence (Figure S5). To further support these results, we generated fusion constructs consisting

of the L6 N-terminal signal anchor (L6s) fused to signaling active RPS4TIR $^{1-235}$ and SNC1TIR $^{1-226}$ to direct these TIR fragments to the Golgi membrane. These constructs both induced cell death responses equivalent to the corresponding constructs without L6s (Figure S6A). Confocal analysis showed that each L6s/TIR-YFP constructs target Golgi bodies (Figures S6 B-E), although some weak YFP fluorescence was also detected in nuclei for L6s/RPS4TIR$^{1-235}$ after infiltration by *Agrobacterium* at OD_{600}=0.5, but not OD_{600}=0.1, which led to lower protein accumulation (Figure S6F). L6s/TIR constructs triggered an immune response that was even stronger than RPS4TIR $^{1-235}$ and SNC1TIR $^{1-226}$ with no signal anchor at OD_{600} 0.1 (Figure 4E) This phenotypical results was validated by ion leakage assays (Figure 4F). Based on our results, we conclude that RPS4 and SNC1 TIR domains can activate cell death signaling from both nuclear and cytosolic compartments in *N. benthamiana.*

Flax L6 can induce cell death responses in Arabidopsis via the cytosolic pool of AtEDS1

EDS1 is required for TNL signaling and displays nucleocytosolic subcellular localization (Parker et al., 1996; Wiermer et al., 2005; Wirthmueller et al., 2007). Our results showing that L6 cannot induce signaling from the nuclear compartment (Figure 2B,C) prompted us to test whether L6 signaling depends on EDS1 subcellular localization. Given that L6 can signal in Arabidopsis (Howles et al., 2005), we generated transgenic lines expressing Dexamethasone (Dex)-inducible full-length L6 autoimmune variant that contains an aspartate to valine substitution in the MHD motif (L6MHV) with a C-terminal 3-myc epitope in Col-0 ecotype. When grown on a non-inducing MS media, seedlings from two independent pDex:L6MHV-3myc transgenic lines showed no developmental differences compared to wild-type Col-0 seedlings (Figures S7 and S8). In contrast, upon transfer on Dex-containing media, seedlings from both transgenic lines died after several days, a phenotype that is typical of an autoimmnune response (Figure S7). We used pDex:L6MHV-3myc line #2 for further characterization. Upon transfer on Dex-containing media, transgenic but not wild-type seedlings, showed chlorotic symptoms from 3 to 4 days after induction (dai), and growth arrest to eventually die by 7/8 dai (Figure 5A). Immunoblot analyses showed that L6MHV-3myc protein only accumulates upon Dex induction (Figure 5B). Hence, this result demonstrates that Dex-induced L6MHV-3myc is functional and triggers immune responses in Arabidopsis. To verify that flax L6MHV initiates signaling via AtEDS1, we crossed our transgenic line with the Col-0 *eds1-2* deletion mutant. In the F2 segregating population of pDex:L6MHV-3myc x *eds1-2*, individual seedlings were selected for the presence of the transgene pDex:L6MHV-3myc (hygromycin selection) and PCR screened to select plants that were homozygous for *eds1-2* mutation (*eds1/eds1*) or which contain a wild-type allele of *EDS1.* When transferred to Dex-inducing media, pDex:L6MHV-3myc x *eds1-2* (*eds1/eds1)* F2 seedlings showed normal development whereas plants with an intact *EDS1* allele

(EDS1/EDS1 or EDS1/*eds1)* were stunted and displayed cell death phenotypes, demonstrating that L6MHV-mediated signaling is dependent on AtEDS1 (Figure S9).

In order to test whether L6 signaling depends on EDS1 subcellular localization, we crossed pDex:L6MHV-3myc/*eds1-2* line with transgenic lines expressing EDS1-YFP or mislocalized EDS1-YFP variants (fused to NLS, NES, nls, or nes sequence under the control of the EDS1 native promotor (pEDS1:EDS1-YFP) in Col-0 *eds1-2* background (García et al., 2010; Stuttmann et al., 2016). For each cross, F3 segregating seedling populations were selected for the presence of the *pDex:L6MHV-3myc* transgene and PCR screened to select individuals that contained the EDS1 variants or not. When transferred to non-inducing (DMSO) media, seedlings from all genotypes showed normal development (Figure S8). Upon transfer to Dex-containing media, seedlings that were not complemented with EDS1-YFP variants also developed normally, similarly to wild-type Col-0 plants (Figure 5A). At 4 dai, seedlings that were complemented with any EDS1-YFP variant showed similar symptoms to the pDex:L6MHV:3myc line that contains the native allele of EDS1, i.e, stunted growth and chlorosis (Figure 5A). By 8 dai, individuals complemented with EDS1-YFP, and EDS1-YFP-NES variants were fully necrotic, similar to individuals from pDex:L6MHV:3myc line. In contrast, individuals from lines complemented with EDS1-YFP-NLS, nls, or nes remained similar to the phenotype observed at 4 dai, and did not die (Figure 5A). Similar results were obtained when pDex:L6MHV:3myc/*eds1-2* line was crossed with independent transgenic lines expressing pEDS1:EDS1-YFP-NLS (#A5) and pEDS1:EDS1-YFP-NES (#2-11) (García et al., 2010; Stuttmann et al., 2016) (Figure S10).

Confocal microscopy of roots of complemented lines (from Figure 5) showed that EDS1-YFP, EDS1-YFP-NLS and EDS1-YFP-NES displayed the expected nucleocytosolic, nuclear restricted or nuclear excluded fluorescence labelling, respectively (Figure S11). In contrast, control variants EDS1-YFP-nls and EDS1-YFP-nes mainly labelled the nuclear compartment, and were lowly expressed compared to the other EDS1-YFP variants, which may explain their lack of complementation.

Immunoblot analysis revealed that 24h after Dex induction, the L6MHV protein accumulates similarly in the pDex:L6MHV-3myc line and in all complemented lines except the one complemented with EDS1-YFP, in which accumulation of the L6MHV protein is slightly reduced (Figure 5B). By using anti-GFP antibodies, we repeatedly observed an increased accumulation of EDS1-YFP variants in seedlings transferred to Dex-containing media, compared to those transferred to non-inducing media, although not identical in every line. However, the level of protein accumulation of EDS1 upon Dex induction do not seem to correlate with the immune response output. Indeed, upon Dex induction, the EDS1-YFP-NLS variant protein accumulation was similar to EDS1-YFP and stronger than EDS1-YFP-NES, which both induce a stronger immune response compared to EDS1-YFP-NLS. Altogether,

it seems that L6MHV signaling leads to seedling death only when EDS1 is present in the cytosolic pool, while nuclear-localised EDS1 is sufficient to mediate the stunting phenotype.

RPS4TIR domain preferentially signals cell death via the cytosolic pool of EDS1 in Arabidopsis

EDS1 is essential for RPS4/RRS1-mediated bacterial immunity in Arabidopsis and for RPS4 TIR signaling in *N. tabacum* and *N. benthamiana* (Wirthmueller et al., 2007; Swiderski et al., 2009; Horsefield et al., 2019). In order to test whether AtEDS1 subcellular localization is important for RPS4TIR signaling, we used the same approach as for L6MHV described above. We generated transgenic lines expressing Dex-inducible RPS4 $^{1-235}$ with a C-terminal FSBP (consisting in a triple Flag tag fused to the streptavidin binding protein(SBP)). When seedlings from three independent lines expressing pDex:RPS4 $^{1-235}$-FSBP were grown on a non-inducing MS media, the *RPS4* $^{1-235}$ transgene was not expressed and seedling development was similar to wild-type Col-0 (Figures S12 and S13). In contrast, when transferred on Dex-containing media, seedlings from all lines died after several days, similarly to pDex:L6MHV-3myc transgenic seedlings (Figure S12). We used RPS4 $^{1-235}$-FSBP line #F for further characterization. Upon transfer on Dex-inducing media, pDex: RPS4 $^{1-235}$-containing seedlings showed chlorotic symptoms from 3 to 4 days after induction , and then growth arrest with fully necrotic symptoms by 6 to 7 dai (Figure 6A), demonstrating that induced RPS4 $^{1-235}$-FSBP is functional and can activate immune responses in Arabidopsis.

In order to test whether RPS4 $^{1-235}$ depends on EDS1 subcellular localization, we introduced the *eds1-2* mutation in the pDex:RPS4 $^{1-235}$-FSBP line and complemented it with EDS1 and mislocalized variants as described above. When transferred to non-inducing (DMSO) media, seedlings from all genotypes showed a normal development, similar to wild-type Col-0 seedlings (Figure S13). Upon transfer on Dex-containing media, pDex:RPS4 $^{1-235}$-FSBP/*eds1-2* seedlings also showed similar development to Col-0 seedlings (Figure 6A), demonstrating that RPS4 $^{1-235}$-FSBP requires EDS1 to signal. At 3 dai, seedlings complemented with any of the EDS1-YFP variants started to show chlorotic symptoms, although seedlings complemented with the EDS1-YFP-NES variant showed slightly stronger autoimmune phenotype that was closer to the pDex: RPS4 $^{1-235}$-FSBP line, i.e. the plantlets were smaller and showed stronger chlorosis symptoms. At 6dai, seedlings from pDex:RPS4 $^{1-235}$-FSBP line complemented with EDS1-YFP-NES were dead, while seedlings from all other lines remained stunted but survived (Figure 6A). Similar results were obtained when pDex: RPS4 $^{1-235}$-FSBP /*eds1-2* line was crossed with independent transgenic lines expressing pEDS1:EDS1-YFP-NLS (#A5) and pEDS1:EDS1-YFP-NES (#2-11) (García et al., 2010; Stuttmann et al., 2016)(Figure S14). Confocal analysis of the complemented lines showed that EDS1 mislocalized variants displayed the expected subcellular localization in these lines, except that EDS1-YFP-nls was again mainly nuclear (Figure S15). Upon Dex induction, RPS4 $^{1-235}$-FSBP protein accumulated at 24hai in all lines (Figure

6B). Similarly to the results obtained with L6MHV, we repeatedly observed an increased accumulation of all EDS1-YFP mislocalized variants upon Dex induction in comparison to non-inducing conditions where RPS4 $^{1-235}$-FSBP is not expressed. The EDS1-YFP and EDS1-YFP-NLS variants showed the highest protein accumulation, but not the strongest autoimmune phenotype (Figure 6B). Thus, similar to Golgi-localized L6MHV, RPS4TIR induction leads to cell death when EDS1 is in the cytosol, with a stunting phenotype without necrosis when EDS1 is restricted to the nucleus.

DISCUSSION

In the last few years, important breakthroughs have revealed the complexity of TIR-containing NLR signaling. However, the subcellular requirement for TNL signaling and downstream immune complexes to activate defense responses is not clearly understood. By studying mislocalized variants of signaling TIR domains isolated from different TNLs, we showed that TNLs do not all activate signaling from the same cellular compartment. Flax L6TIR exclusively signal from the cytosol while Arabidopsis RPS4 and SNC1TIR domains can activate immune signaling from both nuclear and cytosolic compartments in *N. benthamiana.*

TIR-only constructs isolated from Arabidopsis RPS4, SNC1 or flax L6 are not able to trigger signaling, in contrast to larger TIR constructs containing an N-terminal signal anchor for L6 or a C-terminal extension before the start of the NB domain for RPS4 and SNC1. In the case of L6, this may be a consequence of the N-terminal membrane anchor causing concentration of the protein at the Golgi (or tonoplast in the case of the M signal anchor) membrane, thereby promoting self-association. Similarly, fusion of the L6TIR to AvrM, which forms a stable dimer, also promoted signaling in the absence of the membrane anchor. This is consistent with recent data on the requirement of TNL oligomeric assembly to promote TIR self-association to activate NADase catalytic activity (Horsefield et al., 2019; Duxbury et al., 2020; Ma et al., 2020; Martin et al., 2020). As AvrM forms a stable dimer *in planta* (Ve et al., 2013), it is interesting to note that dimerization of L6TIR seems sufficient to activate immune responses.

In contrast, a fusion to AvrM did not induce RPS4 and SNC1 TIR-only signaling. Hence, it is possible that AvrM cannot dimerize or fold properly when fused to RPS4 and SNC1 TIRs, and hence does not promote induced proximity of the TIRs. Interestingly, confinement of RPS4 or SNC1 TIR-alone in the nucleus induced signaling, showing that increasing RPS4 or SNC1 TIR concentration in the nucleus may be sufficient to promote oligomerisation. This is consistent with earlier data showing that increased accumulation of RPS4 or SNC1 full-length protein in the nucleus is sufficient to induce AvrRps4-independent cell death in tobacco or enhanced disease resistance in Arabidopsis,

411 respectively (Wirthmueller et al., 2007; Xu et al., 2014). While interaction with transcriptional
412 corepressor or with DNA in the nucleus suggest that native full length SNC1 and RPS4/RRS1 have
413 nuclear functions (Zhu et al., 2010; Le Roux et al., 2015), our results brings new insights in TNL
414 early signaling as we showed individual TIR domains may have specific subcellular localisation
415 requirements to induce signaling. RPS4 and SNC1 TIR-mediated cell-death signaling can be
416 activated from both nuclear and cytosolic compartments while L6TIR signals in the cytosol but not
417 in the nucleus, highlighting some specificities in TIR domain function and trigger downstream
418 signaling (Sup figure 16).
419 EDS1 is a central regulator of plant immunity and functions downstream of TNL activation. Two
420 recent studies have filled a major gap in how TIR signaling connects to EDS1. The by-products of
421 TIR NADase enzymatic activity act as signaling molecules by binding to and activating EDS1/PAD4
422 or EDS1/SAG101 heterodimers, leading to the association of EDS1 complex to downstream RNL-
423 type helper NLRs and the activation of immune responses (Huang et al., 2022; Jia et al., 2022). By
424 using Arabidopsis transgenic lines conditionally expressing L6MHV, and RPS4TIR$^{1-235}$ in an *eds1*
425 mutant background, we found that autoimmune responses triggered by these two constructs rely on
426 AtEDS1. We also found that L6MHV and RPS4TIR signaling induction enhance AtEDS1 protein
427 accumulation. Increased EDS1 protein accumulation was also observed in the *snc1* autoimmune
428 mutant compared to wild-type plants (García et al., 2010), supporting a direct connection between
429 TIR signaling and EDS1 accumulation. Indeed, TIR-catalysed small molecules may stabilize the
430 EDS1 protein and/or upregulate *EDS1* transcription. Here, we showed that only the cytosolic pool of
431 AtEDS1 can translate signaling from nucleocytosolic RPS4TIR $^{1-235}$ and from Golgi membrane-
432 anchored flax L6MHV to a cell death response. However, plants expressing nuclear-restricted EDS1
433 still showed a stunting phenotype but remained alive, indicating that some aspects of immune
434 signaling can also be mediated by the nuclear fraction of EDS1, even when the inducing TIR is
435 confined to the cytosolic space in the case of the Golgi-localised L6MHV (Sup figure 16). This result
436 is consistent with earlier observations that nuclear EDS1 is essential for TNL-mediated resistance
437 and transcriptional reprogramming while the cytosolic pool is involved in cell death activation
438 (García et al., 2010; Bhandari et al., 2019; Lapin et al., 2019). Interestingly, restricting EDS1 to the
439 nuclear compartment do not prevent TNL RPP4-mediated hypersensitive response (localized cell
440 death) upon infection with avirulent *Hyaloperonospora arabidopsidis* in Arabidopsis (Stuttmann et
441 al., 2016). It is possible that the activation of effector-independent TIR signaling (inducible
442 expression in transgenic lines) may differ from pathogen-delivered effector-mediated TNL activation.
443 Given evidence of cross-talk between PTI and ETI this may explain the discrepancy (Bernoux et al.,
444 2022).

Previous studies suggest that the EDS1/PAD4/ADR1 module controls pathogen restriction whereas EDS1/SAG101/NRG1 activate cell death (Lapin et al., 2019).

Interestingly, AtSAG101 was found to be nuclear localized upon transient expression in *N. benthamiana* leaves Arabidopsis (Lapin et al. 2019). However, this may not reflect its normal distribution as part of an EDS1-SAG101 complex as the Arabidopsis SAG101 does not function with the *N. benthamiana* EDS1 protein.

. A recent study reported the formation of a complex between the EDS1-SAG101 module and NRG1 in both nuclei and at the plasma membrane, nevertheless the stoichiometry of these complexes seemed different in the nucleus and may explain functional differences (Feehan et al., 2022). Nuclear complexes seem to form heterotrimers while larger resistosome-like structures associate with the plasma membrane. Hence, nuclear restricted EDS1 may be able to associate with SAG101 and NRG1 to activate an immune response in the nucleus, but is not able to further induce the formation of a pore-forming resistosome to induce cell death in the cytosol.

Nuclear export signal leads to enhanced nuclear export but does not fully prevent nuclear import. Hence, it is possible that brief nuclear import of EDS1-YFP^{NES} to the nucleus is sufficient to interact with nuclear SAG101 and activate NRG1 to trigger cell death at the plasma membrane. The contribution of the EDS1/PAD4/ADR1 to transcriptional reprogramming vs cell death execution remains unclear as EDS1 and PAD4 both shuttles to the nucleus and the cytosol while ADR1s are mainly targeted to the plasma membrane (Saile et al., 2021). Studying the subcellular dynamics of all signaling partners upon TNL activation needs to be thoroughly addressed to fully understand the roles of EDS1/SAG101/NRG1 vs EDS1/PAD4/ADR1 modules and how they differentially engage into cell death or resistance/gene reprogramming pathways.

How nuclear-restricted EDS1 senses cytosolic TIR signaling activity such as from Golgi-localized L6MHV is unclear but may be explained by the diffusion of TIR-catalysed molecules through the nuclear envelope to activate EDS1. On the other hand, it is possible that EDS1-YFP-NLS is weakly expressed in the cytosol or encounters Golgi localised L6MHV during protein translation and that this is sufficient to activate signaling in the early stages after Dex induction, explaining why cell death symptoms slow down after a few days after Dex induction. NLR-mediated immune responses lead to core-immunity gene reprogramming, including upregulation of *TNLs* (Bernoux et al., 2022). Hence, it is also possible that L6MHV induces rapid expression of *TNLs*, some of which proteins may be targeted to the nucleus and activate nuclear restricted EDS1. Lastly, we cannot exclude that the other members of the EDS1 family (PAD4 and SAG101) can sense cytosolic TIR-catalysed signaling molecule and shuttle between the cytoplasm and nucleus to translate the signal to nuclear-restricted EDS1. Indeed, we recently obtained evidence that TIR proteins can interact with all members of the

EDS1 family in *N. benthamiana* and in yeast, independently or as heterodimers (Chen et al., in preparation).

Interestingly, the nuclear pool of SlEDS1 and SlSAG101 is required and sufficient for effector-triggered Roq1-mediated cell death in *N. benthamiana* (Zönnchen et al., 2022). In contrast, the cytosolic pool of AtEDS1 and AtSAG101 can activate Roq1-mediated cell death (Wang et al. 2023), suggesting that NLR signaling and subcellular requirements may not be conserved across species. . Investigating the specificities and commonalities of NLR activation and signaling in other plant species will be crucial for improving disease resistance in crops.

EXPERIMENTAL PROCEDURES

Vectors and plasmid construction

All DNA plasmids and primers used in this study are listed in Supplemental table 1 and 2. Plasmids for *in planta* transient expression were constructed by Gateway cloning (GWY; Invitrogen). PCR products flanked by the attB sites were recombined into pDONR207 (Invitrogen) and then into corresponding destination vectors: pAM-PAT 35S:GWY-YFPv (Bernoux et al., 2008), pAM-PAT 35S:GWY-AvrM, pAM-PAT 35S:GWY-YFPv-NLS/nls (Cesari et al., 2016), pAM-PAT 35S:GWY-YFPv-NES/nes, pAM-PAT 35S:GWY-AvrM-YFPv-NLS/NES series, pDex:GWY-3myc or pDex:GWY-FSBP.

To generate pAM-PAT-35S:GWY-YFPv-NES/nes, *SmaI/XbaI* PCR fragments containing the YFPv sequence with a functional NES sequence from HIV Rev (LQLPPLERLTL) or a non-functional nes (LQAPPAERATL)(Wen et al., 1995) at the C-terminal end of the YFP, were ligated into pAM-PAT 35S:GWY-YFPv digested with *SmaI* and *XbaI* to excise and replace the orginal YFPv fragment. The pAM-PAT 35S:GWY-AvrM was generated in a 2-step process by fusing two PCR fragments with overlapping sequence and ligation into pAM-PAT 35S:GWY-YFPv digested with *PstI* and *XbaI* to dislodge and replace the orginal YFPv. PCR fragment 1 was generated to contain the 3'end of the GWY cassette sequence of the PAM-PAT-GWY-YFP (with a 5' Pst1 restriction site), up to the AttR2 sequence. PCR fragment 2 was generated to amplify AvrM-A sequence with a 3' *XbaI* site and overlapping sequence with PCR fragment 1 in its 5'end. The two PCR fragments containing overlapping sequence in their 3' and 5', respectively, were assembled by PCR and then ligated into pAM-PAT 35S:GWY-YFPv digested with *PstI* and *XbaI* to dislodge and replace the orginal YFPv fragment. pAM-PAT 35S:GWY-AvrM-YFP-NLS/NES plasmid series were also generated in a 2-step PCR process. Two PCR fragments containing AvrM-A with a 5' *PstI* restriction site and another one containing YFPv-NLS/NES/nls/nes with a 3' *XbaI* restriction site and an overlapping linker sequence (GGSGG) in their 3' and 5' end, respectively were assembled by PCR and then ligated into

pAM-PAT 35S:GWY-YFPv digested with *PstI* and *XbaI* to dislodge and replace the original YFPv. The L6 signal anchor (L6s, residues 1-58) was inserted into the *XhoI* and *HindIII* sites of the pAM-PAT 35s:GWY-YFP vector upstream the AttR1 site to generate the pAM-PAT 35s: L6s-GWY-YFP. pDex:GWY-3Myc and pDex:GWY-FSBP were modified from pOpOff2(Hyg) -derived vectors (Craft et al., 2005; Wielopolska et al., 2005). pOpOff2(Hyg) GWY-derived vector, was kindly provided by Chris Helliwell (CSIRO, Canberra). It was lacking the hairpin GWY cassette (as described in (Wielopolska et al., 2005)) and instead contained a simple GWY cassette but no terminator. Hence, a PCR fragment containing either a triple myc or the FSBP (3xFLAG-streptavidin binding protein) epitopes followed by the 35s terminator sequence flanked with *KpnI* restriction sites, were cloned into pOpOff2(Hyg)-derived vector digested with Kpn1. All plasmids and constructs were verified by sequencing. Details of constructs and primers used in this study are listed in Supplemental table 1 and 2.

Plant material

Nicotiana benthamiana and *N. tabacum* W38 plants were grown in growth chambers at 21°C under 9h photoperiod. *A. thaliana* seeds were sown on MS (Murashige and Skoog) media, vernalized for 24 h and transferred in growth chambers for ten days under 22°C and 16h photoperiod conditions.

Arabidopsis crosses and PCR screening

Transgenic lines expressing pDex:L6MHV-3myc (line #2) or pDex:RPS4 $^{1-235}$-FSBP (line#F) were selected on MS media supplemented with hygromycin 15 µg/ml, and crossed with Col-0 *eds1-2* deletion mutant. F2 segregating seedling population were selected for the presence of the transgene (hygromycin selection) and individually PCR screened to check for the presence of the *EDS1* deletion by using Thermo Scientific™ Phire plant direct PCR kit. In brief, the first emerging leaf of 10 day-old of individual seedling was sampled and ground in 10µl extraction buffer provided by the kit. 0.5µl of this extract was then used to run a PCR, following the manufacturer recommendations, with primers located on each side of the deletion in *EDS1* (EDS1 F563/ EDS1 R1806) *(*Supplemental table 2). Individuals carrying pDex transgene and homozygous *eds1-2* deletion (pDex:L6MHV-3myc x *eds1-2* line #4.5 and pDex:RPS4 $^{1-235}$-FSBP x *eds1-2* line #8.1) were crossed with lines expressing mislocalized variants of EDS1 (pEDS1:EDS1-YFP fused to nuclear localization signal (NLS), nuclear exclusion signal (NES) or corresponding mutants (nls, nes), pEDS1:EDS1-YFP-NLS#B2, pEDS1:EDS1-YFP-NLS#A5, pEDS1:EDS1-YFP-NES#3-4, pEDS1:EDS1-YFP-NES#2-11, pEDS1:EDS1-YFP-nls#B5, pEDS1:EDS1-YFP-nes#1-2 (García et al., 2010; Stuttmann et al., 2016). Arabidopsis F3 segregating populations were individually PCR screened to select individual

549 seedlings that were homozygous for *eds1-2* mutation (*eds1/eds1*) or contained the EDS1 mislocalized
550 variants for cell death assays, confocal microscopy and western-blots analyses.
551
552 **Agrobacterium-mediated transient expression in flax and tobacco**
553 *Agrobacterium tumefaciens* cells were grown for 24h at 28°C in LB medium containing appropriate
554 antibiotics selection. Cells were pelleted, resuspended in the infiltration medium (10 mM $MgCl_2$,
555 10mM MES PH5,6, 150 µM acetosyringone), adjusted to OD_{600} = 1, 0.5 or 0.1 before infiltration into
556 leaves of 4 week-old flax (Hoshangabad) or OD_{600} =0.5 or 0.1 into leaves of 4 week-old *Nicotiana*
557 *benthamiana*.
558
559 **Dexamethasone induction and cell death assay in *Arabidopsis thaliana***
560 Ten day-old seedlings were transferred on MS media supplemented with dexamethasone (10µM) or
561 DMSO (equivalent volume as dexamethasone) and left in growth chambers under 22°C and 16 h
562 photoperiod conditions. The apparition of cell death symptoms were monitored every day. For
563 immunoblot analysis, five seedlings per sample were collected 24h after induction.
564
565 **Immunoblot analysis**
566 Total proteins were extracted by grinding two flax leaves or two *N. benthamiana* leaf discs (1cm
567 diameter), three days and two days after agroinfiltration, respectively. Plant material was resuspended
568 in 100 µL of loading Laemmli buffer. Total proteins of Arabidopsis were extracted by grinding five
569 ten day-old seedlings 24h after Dex-induction, in 100µl of protein extraction buffer (150mM Tris-
570 HCl pH 7.5, 150mMNaCl, 1mM EDTA, 1%NP40, 1% plant protease inhibitor cocktail
571 (SIGMA),10mM DTT, 10µM MG132). Protein lysates were centrifuged to remove cell debris and
572 50µl of supernatant was combined with 50µl of loading Laemmli buffer. All protein samples were
573 denatured at 95°C for three minutes before loading on SDS-PAGE and transfer to nitrocellulose
574 membrane. Membranes were blocked in 5% skim milk and probed with anti-Flag-HRP (Sigma,
575 A8592), anti-c-myc-peroxidase (clone 9E10, Roche) or anti-GFP mouse monoclonal antibodies
576 (clones 7.1 and 13.1, Roche, Ref#11814460001, Lot 13921700), followed by goat anti-mouse HRP
577 conjugate (Bio-Rad, Cat#170-5047). Proteins were revealed using BioRad Chemidoc™ Imaging
578 system with the Bio-Rad Western ECL Substrate. Membranes were stained with Red Ponceau to
579 verify protein loading.
580
581 **Measurement of ion leakage from leaf discs**
582 Ion leakage measurements were performed as in (Zhang et al., 2017b). Briefly, for each construct,
583 four leaf discs (0.9 cm diameter) of *N. benthamiana* leaves were sampled 48h after agroinfiltration,

quickly rinsed with distilled water and incubated for 24h with 1.8ml of fresh MilliQ water. Conductivity of the bathing solution was measured before (C1) and after (C2) boiling for 10 minutes to release the total ion content of the leaf discs, by using a Horiba B-173 conductivity meter. Ion leakage was expressed as C1/C2 ratio.

Confocal microscopy

Confocal fluorescence images were recorded on a Leica SP8 confocal system, using 514-nm laser line to image YFP signal. In *A. thaliana*, roots of 10 week-old Arabidopsis seedlings were analysed 24h after Dexamethasone induction. In *N. benthamiana*, leaf discs were analysed 48h after infiltration with *A. tumefaciens*.

DATA AVAILABILITY STATEMENT

All relevant data can be found within the manuscript and its supporting materials.

ACKNOWLEDGEMENTS

Dexamethasone-inducible pOpOff2-derived vectors used to generate pDex:GWY-3myc and pDex:GWY-FSBP were kindly provided by Dr Chris Helliwell (CSIRO Canberra, Australia).

Col-0 *eds1-2 and* Col-0 *eds1-2 lines* complemented with EDS1-YFP mislocalized variants were kindly provided by Prof. Jane E. Parker (Max Planck Institute, Cologne, Germany).

This work was supported by the Australian research council (ARC), Discovery Early Career Research Awards (DE130101292) awarded to MB. This research was set within the framework of the "Laboratoires d'Excellence (LABEX)" TULIP (ANR-10-LABX-41) and of the "École Universitaire de Recherche (EUR)" TULIP-GS (ANR-18-EURE-0019) [MB]. JC was supported by a Chinese Scholarship Council (CSC) postgraduate fellowship.

AUTHOR CONTRIBUTIONS

MB and PD initiated the project and designed the experiments, MB, JC, XZ, KN and JH performed experiments. MB, JC, XZ, and PD analysed the data. MB wrote the manuscript with the contributions of PD, JC, XZ and LD.

CONFLICT OF INTERESTS

The authors declare there are no conflict of interests.

SUPPORTING INFORMATION

Figure S1. Signalling activity, and protein stability of mislocalized variants of P2/L6TIR.

Figure S2. Signalling activity of membrane-tethered L6 TIR is not affected by a fusion to AvrM and a nuclear localization or nuclear exclusion signal.

Figure S3. Subcellular localization of RPS4 and SNC1 TIR constructs.

Figure S4. Subcellular localization of mislocalized variants of RPS4 and SNC1 TIR-only.

Figure S5. Subcellular localization of mislocalized variants of RPS4 $^{1-235}$ and SNC1 $^{1-226}$ TIR constructs.

Figure S6. Signaling activity, subcellular localization and protein accumulation of RPS4 $^{1-235}$ and SNC1 $^{1-226}$ TIR constructs fused to L6 signal anchor.

Figure S7. Phenotype of independent transgenic Arabidopsis seedlings expressing Dexamethasone (Dex)-inducible L6MHV-3myc (pDex:L6MHV-3myc).

Figure S8. Phenotype of transgenic Arabidopsis seedlings expressing pDex:L6MHV on a non-inducing media.

Figure S9. Flax L6 signaling in Arabidopsis depends on AtEDS1.

Figure S10. Phenotype of transgenic Arabidopsis seedlings from crosses of pDex:L6MHV-3myc/*eds1-2* line with independent mislocalized EDS1 variants lines.

Figure S11. Subcellular localization of EDS1-YFP variants in Dex-inducible transgenic Arabidopsis seedlings (10 day-old) expressing pDex:L6MHV in *eds1-2* mutant background complemented with mislocalized EDS1-YFP variants.

Figure S12. Phenotype of independent transgenic Arabidopsis seedlings expressing Dexamethasone (Dex)-inducible RPS4 $^{1-235}$-FSBP.

Figure S13. Phenotype of transgenic Arabidopsis seedlings expressing pDex:RPS4 $^{1-235}$ on a non-inducing media.

Figure S14. Phenotype of transgenic Arabidopsis seedlings from crosses of pDex: RPS4 $^{1-235}$-FSBP /*eds1-2* line #8.1 with independent mislocalized EDS1 variants lines.

Figure S15. Subcellular localization of EDS1-YFP variants in Dex-inducible transgenic Arabidopsis seedlings (10 day-old) expressing pDex:RPS4 $^{1-235}$ in *eds1-2* mutant background complemented with mislocalized EDS1-YFP variants.

Figure S16. TIR signaling subcellular localization requirement model.

REFERENCES

Bentham, A., Burdett, H., Anderson, P.A., Williams, S.J., and Kobe, B. (2016). Animal NLRs provide structural insights into plant NLR function. Ann Bot.

Bernoux, M., Zetzsche, H., and Stuttmann, J. (2022). Connecting the dots between cell surface- and intracellular-triggered immune pathways in plants. Curr Opin Plant Biol **69,** 102276.

Bernoux, M., Timmers, T., Jauneau, A., Briere, C., de Wit, P.J., Marco, Y., and Deslandes, L. (2008). RD19, an Arabidopsis cysteine protease required for RRS1-R-mediated resistance, is relocalized to the nucleus by the Ralstonia solanacearum PopP2 effector. Plant Cell **20,** 2252-2264.

Bernoux, M., Ve, T., Williams, S., Warren, C., Hatters, D., Valkov, E., Zhang, X., Ellis, J.G., Kobe, B., and Dodds, P.N. (2011). Structural and functional analysis of a plant resistance protein TIR domain reveals interfaces for self-association, signaling, and autoregulation. Cell Host Microbe **9,** 200-211.

Bernoux, M., Burdett, H., Williams, S.J., Zhang, X., Chen, C., Newell, K., Lawrence, G.J., Kobe, B., Ellis, J.G., Anderson, P.A., and Dodds, P.N. (2016). Comparative Analysis of the Flax Immune Receptors L6 and L7 Suggests an Equilibrium-Based Switch Activation Model. Plant Cell **28,** 146-159.

Bhandari, D.D., Lapin, D., Kracher, B., von Born, P., Bautor, J., Niefind, K., and Parker, J.E. (2019). An EDS1 heterodimer signalling surface enforces timely reprogramming of immunity genes in Arabidopsis. Nat Commun **10,** 772.

Bhattacharjee, S., Halane, M.K., Kim, S.H., and Gassmann, W. (2011). Pathogen effectors target Arabidopsis EDS1 and alter its interactions with immune regulators. Science **334,** 1405-1408.

Bi, G., Su, M., Li, N., Liang, Y., Dang, S., Xu, J., Hu, M., Wang, J., Zou, M., Deng, Y., Li, Q., Huang, S., Li, J., Chai, J., He, K., Chen, Y.H., and Zhou, J.M. (2021). The ZAR1 resistosome is a calcium-permeable channel triggering plant immune signaling. Cell **184,** 3528-3541.e3512.

Catanzariti, A.M., Dodds, P.N., Lawrence, G.J., Ayliffe, M.A., and Ellis, J.G. (2006). Haustorially expressed secreted proteins from flax rust are highly enriched for avirulence elicitors. Plant Cell **18,** 243-256.

Catanzariti, A.M., Dodds, P.N., Ve, T., Kobe, B., Ellis, J.G., and Staskawicz, B.J. (2010). The AvrM effector from flax rust has a structured C-terminal domain and interacts directly with the M resistance protein. Mol Plant Microbe Interact **23,** 49-57.

Cesari, S., Moore, J., Chen, C., Webb, D., Periyannan, S., Mago, R., Bernoux, M., Lagudah, E.S., and Dodds, P.N. (2016). Cytosolic activation of cell death and stem rust resistance by cereal MLA-family CC-NLR proteins. Proc Natl Acad Sci U S A **113,** 10204-10209.

Cheng, Y.T., Germain, H., Wiermer, M., Bi, D., Xu, F., García, A.V., Wirthmueller, L., Després, C., Parker, J.E., Zhang, Y., and Li, X. (2009). Nuclear pore complex component MOS7/Nup88 is required for innate immunity and nuclear accumulation of defense regulators in Arabidopsis. Plant Cell **21,** 2503-2516.

Craft, J., Samalova, M., Baroux, C., Townley, H., Martinez, A., Jepson, I., Tsiantis, M., and Moore, I. (2005). New pOp/LhG4 vectors for stringent glucocorticoid-dependent transgene expression in Arabidopsis. Plant J **41,** 899-918.

Dodds, P.N., and Rathjen, J.P. (2010). Plant immunity: towards an integrated view of plant-pathogen interactions. Nat Rev Genet **11,** 539-548.

Dodds, P.N., Lawrence, G.J., Catanzariti, A.M., Teh, T., Wang, C.I., Ayliffe, M.A., Kobe, B., and Ellis, J.G. (2006). Direct protein interaction underlies gene-for-gene specificity and coevolution of the flax resistance genes and flax rust avirulence genes. Proc Natl Acad Sci U S A **103,** 8888-8893.

Dong, O.X., Tong, M., Bonardi, V., El Kasmi, F., Woloshen, V., Wunsch, L.K., Dangl, J.L., and Li, X. (2016). TNL-mediated immunity in Arabidopsis requires complex regulation of the redundant ADR1 gene family. New Phytol **210,** 960-973.

Duxbury, Z., Ma, Y., Furzer, O.J., Huh, S.U., Cevik, V., Jones, J.D., and Sarris, P.F. (2016). Pathogen perception by NLRs in plants and animals: Parallel worlds. Bioessays **38,** 769-781.

Duxbury, Z., Wang, S., MacKenzie, C.I., Tenthorey, J.L., Zhang, X., Huh, S.U., Hu, L., Hill, L., Ngou, P.M., Ding, P., Chen, J., Ma, Y., Guo, H., Castel, B., Moschou, P.N., Bernoux, M., Dodds, P.N., Vance, R.E., and Jones, J.D.G. (2020). Induced proximity of a TIR signaling domain on a plant-mammalian NLR chimera activates defense in plants. Proc Natl Acad Sci U S A **117,** 18832-18839.

Essuman, K., Milbrandt, J., Dangl, J.L., and Nishimura, M.T. (2022). Shared TIR enzymatic functions regulate cell death and immunity across the tree of life. Science **377,** eabo0001.

Feehan, J.M., Wang, J., Sun, X., Choi, J., iew ORCID Profile Ahn, H.-K., Ngou, B.P.M., Parker, J.E., and Jones, J.D.G. (2023). Oligomerization of a plant helper NLR requires cell-surface and intracellular immune receptor activation, Proc Natl Acad Sci U S A, **120**, e2210406120

Förderer, A., Li, E., Lawson, A.W., Deng, Y.N., Sun, Y., Logemann, E., Zhang, X., Wen, J., Han, Z., Chang, J., Chen, Y., Schulze-Lefert, P., and Chai, J. (2022). A wheat resistosome defines common principles of immune receptor channels. Nature.

García, A.V., Blanvillain-Baufumé, S., Huibers, R.P., Wiermer, M., Li, G., Gobbato, E., Rietz, S., and Parker, J.E. (2010). Balanced nuclear and cytoplasmic activities of EDS1 are required for a complete plant innate immune response. PLoS Pathog **6,** e1000970.

Gerdts, J., Brace, E.J., Sasaki, Y., DiAntonio, A., and Milbrandt, J. (2015). SARM1 activation triggers axon degeneration locally via NAD^+ destruction. Science **348,** 453-457.

Heidrich, K., Wirthmueller, L., Tasset, C., Pouzet, C., Deslandes, L., and Parker, J.E. (2011). Arabidopsis EDS1 connects pathogen effector recognition to cell compartment-specific immune responses. Science **334,** 1401-1404.

Horsefield, S., Burdett, H., Zhang, X., Manik, M.K., Shi, Y., Chen, J., Qi, T., Gilley, J., Lai, J.S., Rank, M.X., Casey, L.W., Gu, W., Ericsson, D.J., Foley, G., Hughes, R.O., Bosanac, T., von Itzstein, M., Rathjen, J.P., Nanson, J.D., Boden, M., Dry, I.B., Williams, S.J., Staskawicz, B.J., Coleman, M.P., Ve, T., Dodds, P.N., and Kobe, B. (2019). NAD + cleavage activity by animal and plant TIR domains in cell death pathways. Science **365,** 793-799.

Howles, P., Lawrence, G., Finnegan, J., McFadden, H., Ayliffe, M., Dodds, P., and Ellis, J. (2005). Autoactive alleles of the flax L6 rust resistance gene induce non-race-specific rust resistance associated with the hypersensitive response. Mol Plant Microbe Interact **18,** 570-582.

Huang, S., Jia, A., Song, W., Hessler, G., Meng, Y., Sun, Y., Xu, L., Laessle, H., Jirschitzka, J., Ma, S., Xiao, Y., Yu, D., Hou, J., Liu, R., Sun, H., Liu, X., Han, Z., Chang, J., Parker, J.E., and Chai, J. (2022). Identification and receptor mechanism of TIR-catalyzed small molecules in plant immunity. Science **377,** eabq3297.

Huh, S.U., Cevik, V., Ding, P., Duxbury, Z., Ma, Y., Tomlinson, L., Sarris, P.F., and Jones, J.D.G. (2017). Protein-protein interactions in the RPS4/RRS1 immune receptor complex. PLoS Pathog **13,** e1006376.

Jacob, P., Kim, N.H., Wu, F., El-Kasmi, F., Chi, Y., Walton, W.G., Furzer, O.J., Lietzan, A.D., Sunil, S., Kempthorn, K., Redinbo, M.R., Pei, Z.M., Wan, L., and Dangl, J.L. (2021). Plant "helper" immune receptors are Ca. Science.

Jia, A., Huang, S., Song, W., Wang, J., Meng, Y., Sun, Y., Xu, L., Laessle, H., Jirschitzka, J., Hou, J., Zhang, T., Yu, W., Hessler, G., Li, E., Ma, S., Yu, D., Gebauer, J., Baumann, U., Liu, X., Han, Z., Chang, J., Parker, J.E., and Chai, J. (2022). TIR-catalyzed ADP-

ribosylation reactions produce signaling molecules for plant immunity. Science **377,** eabq8180.

Kim, T.H., Kunz, H.H., Bhattacharjee, S., Hauser, F., Park, J., Engineer, C., Liu, A., Ha, T., Parker, J.E., Gassmann, W., and Schroeder, J.I. (2012). Natural variation in small molecule-induced TIR-NB-LRR signaling induces root growth arrest via EDS1- and PAD4-complexed R protein VICTR in Arabidopsis. Plant Cell **24,** 5177-5192.

Lapin, D., Bhandari, D.D., and Parker, J.E. (2020). Origins and Immunity Networking Functions of EDS1 Family Proteins. Annu Rev Phytopathol **58,** 253-276.

Lapin, D., Kovacova, V., Sun, X., Dongus, J.A., Bhandari, D., von Born, P., Bautor, J., Guarneri, N., Rzemieniewski, J., Stuttmann, J., Beyer, A., and Parker, J.E. (2019). A Coevolved EDS1-SAG101-NRG1 Module Mediates Cell Death Signaling by TIR-Domain Immune Receptors. Plant Cell **31,** 2430-2455.

Le Roux, C., Huet, G., Jauneau, A., Camborde, L., Tremousaygue, D., Kraut, A., Zhou, B., Levaillant, M., Adachi, H., Yoshioka, H., Raffaele, S., Berthome, R., Coute, Y., Parker, J.E., and Deslandes, L. (2015). A receptor pair with an integrated decoy converts pathogen disabling of transcription factors to immunity. Cell **161,** 1074-1088.

Lu, Y., and Tsuda, K. (2021). Intimate Association of PRR- and NLR-Mediated Signaling in Plant Immunity. Mol Plant Microbe Interact **34,** 3-14.

Lüdke, D., Yan, Q., Rohmann, P.F.W., and Wiermer, M. (2022). NLR we there yet? Nucleocytoplasmic coordination of NLR-mediated immunity. New Phytol.

Ma, S., Lapin, D., Liu, L., Sun, Y., Song, W., Zhang, X., Logemann, E., Yu, D., Wang, J., Jirschitzka, J., Han, Z., Schulze-Lefert, P., Parker, J.E., and Chai, J. (2020). Direct pathogen-induced assembly of an NLR immune receptor complex to form a holoenzyme. Science **370**.

Martin, R., Qi, T., Zhang, H., Liu, F., King, M., Toth, C., Nogales, E., and Staskawicz, B.J. (2020). Structure of the activated ROQ1 resistosome directly recognizing the pathogen effector XopQ. Science **370**.

Parker, J.E., Holub, E.B., Frost, L.N., Falk, A., Gunn, N.D., and Daniels, M.J. (1996). Characterization of eds1, a mutation in Arabidopsis suppressing resistance to Peronospora parasitica specified by several different RPP genes. Plant Cell **8,** 2033-2046.

Saile, S.C., Jacob, P., Castel, B., Jubic, L.M., Salas-Gonzáles, I., Bäcker, M., Jones, J.D.G., Dangl, J.L., and El Kasmi, F. (2020). Two unequally redundant "helper" immune receptor families mediate Arabidopsis thaliana intracellular "sensor" immune receptor functions. PLoS Biol **18,** e3000783.

Saile, S.C., Ackermann, F.M., Sunil, S., Keicher, J., Bayless, A., Bonardi, V., Wan, L., Doumane, M., Stöbbe, E., Jaillais, Y., Caillaud, M.C., Dangl, J.L., Nishimura, M.T., Oecking, C., and El Kasmi, F. (2021). Arabidopsis ADR1 helper NLR immune receptors localize and function at the plasma membrane in a phospholipid dependent manner. New Phytol **232,** 2440-2456.

Sarris, P.F., Duxbury, Z., Huh, S.U., Ma, Y., Segonzac, C., Sklenar, J., Derbyshire, P., Cevik, V., Rallapalli, G., Saucet, S.B., Wirthmueller, L., Menke, F.L., Sohn, K.H., and Jones, J.D. (2015). A Plant Immune Receptor Detects Pathogen Effectors that Target WRKY Transcription Factors. Cell **161,** 1089-1100.

Stuttmann, J., Peine, N., Garcia, A.V., Wagner, C., Choudhury, S.R., Wang, Y., James, G.V., Griebel, T., Alcazar, R., Tsuda, K., Schneeberger, K., and Parker, J.E. (2016). Arabidopsis thaliana DM2h (R8) within the Landsberg RPP1-like Resistance Locus Underlies Three Different Cases of EDS1-Conditioned Autoimmunity. PLoS Genet **12,** e1005990.

Swiderski, M.R., Birker, D., and Jones, J.D. (2009). The TIR domain of TIR-NB-LRR resistance proteins is a signaling domain involved in cell death induction. Mol Plant Microbe Interact **22,** 157-165.

Takemoto, D., Rafiqi, M., Hurley, U., Lawrence, G.J., Bernoux, M., Hardham, A.R., Ellis, J.G., Dodds, P.N., and Jones, D.A. (2012). N-terminal motifs in some plant disease resistance proteins function in membrane attachment and contribute to disease resistance. Mol Plant Microbe Interact **25,** 379-392.

Ve, T., Williams, S.J., and Kobe, B. (2015). Structure and function of Toll/interleukin-1 receptor/resistance protein (TIR) domains. Apoptosis **20,** 250-261.

Ve, T., Williams, S.J., Catanzariti, A.M., Rafiqi, M., Rahman, M., Ellis, J.G., Hardham, A.R., Jones, D.A., Anderson, P.A., Dodds, P.N., and Kobe, B. (2013). Structures of the flax-rust effector AvrM reveal insights into the molecular basis of plant-cell entry and effector-triggered immunity. Proc Natl Acad Sci U S A **110,** 17594-17599.

Wan, L., Essuman, K., Anderson, R.G., Sasaki, Y., Monteiro, F., Chung, E.H., Osborne Nishimura, E., DiAntonio, A., Milbrandt, J., Dangl, J.L., and Nishimura, M.T. (2019). TIR domains of plant immune receptors are NAD. Science **365,** 799-803.

Wang, J., Hu, M., Qi, J., Han, Z., Wang, G., Qi, Y., Wang, H.W., Zhou, J.M., and Chai, J. (2019a). Reconstitution and structure of a plant NLR resistosome conferring immunity. Science **364**.

Wang, J., Hu, M., Wu, S., Qi, J., Wang, G., Han, Z., Qi, Y., Gao, N., Wang, H.W., Zhou, J.M., and Chai, J. (2019b). Ligand-triggered allosteric ADP release primes a plant NLR complex. Science **364**.

Wen, W., Meinkoth, J.L., Tsien, R.Y., and Taylor, S.S. (1995). Identification of a signal for rapid export of proteins from the nucleus. Cell **82,** 463-473.

Wielopolska, A., Townley, H., Moore, I., Waterhouse, P., and Helliwell, C. (2005). A high-throughput inducible RNAi vector for plants. Plant Biotechnol J **3,** 583-590.

Wiermer, M., Feys, B.J., and Parker, J.E. (2005). Plant immunity: the EDS1 regulatory node. Curr Opin Plant Biol **8,** 383-389.

Williams, S.J., Sohn, K.H., Wan, L., Bernoux, M., Sarris, P.F., Segonzac, C., Ve, T., Ma, Y., Saucet, S.B., Ericsson, D.J., Casey, L.W., Lonhienne, T., Winzor, D.J., Zhang, X., Coerdt, A., Parker, J.E., Dodds, P.N., Kobe, B., and Jones, J.D. (2014). Structural basis for assembly and function of a heterodimeric plant immune receptor. Science **344,** 299-303.

Wirthmueller, L., Zhang, Y., Jones, J.D., and Parker, J.E. (2007). Nuclear accumulation of the Arabidopsis immune receptor RPS4 is necessary for triggering EDS1-dependent defense. Curr Biol **17,** 2023-2029.

Wu, Z., Li, M., Dong, O.X., Xia, S., Liang, W., Bao, Y., Wasteneys, G., and Li, X. (2019). Differential regulation of TNL-mediated immune signaling by redundant helper CNLs. New Phytol **222,** 938-953.

Xu, F., Cheng, Y.T., Kapos, P., Huang, Y., and Li, X. (2014). P-loop-dependent NLR SNC1 can oligomerize and activate immunity in the nucleus. Mol Plant **7,** 1801-1804.

Yu, D., Song, W., Tan, E.Y.J., Liu, L., Cao, Y., Jirschitzka, J., Li, E., Logemann, E., Xu, C., Huang, S., Jia, A., Chang, X., Han, Z., Wu, B., Schulze-Lefert, P., and Chai, J. (2022). TIR domains of plant immune receptors are 2',3'-cAMP/cGMP synthetases mediating cell death. Cell **185,** 2370-2386.e2318.

Zhang, X., Dodds, P.N., and Bernoux, M. (2017a). What Do We Know About NOD-Like Receptors in Plant Immunity? Annu Rev Phytopathol **55,** 205-229.

Zhang, X., Bernoux, M., Bentham, A.R., Newman, T.E., Ve, T., Casey, L.W., Raaymakers, T.M., Hu, J., Croll, T.I., Schreiber, K.J., Staskawicz, B.J., Anderson, P.A., Sohn, K.H., Williams, S.J., Dodds, P.N., and Kobe, B. (2017b). Multiple functional self-association interfaces in plant TIR domains. Proc Natl Acad Sci U S A **114,** E2046-E2052.

Zhang, Y., Song, G., Lal, N.K., Nagalakshmi, U., Li, Y., Zheng, W., Huang, P.J., Branon, T.C., Ting, A.Y., Walley, J.W., and Dinesh-Kumar, S.P. (2019). TurboID-based proximity labeling reveals that UBR7 is a regulator of N NLR immune receptor-mediated immunity. Nat Commun **10,** 3252.

Zhu, Z., Xu, F., Zhang, Y., Cheng, Y.T., Wiermer, M., and Li, X. (2010). Arabidopsis resistance protein SNC1 activates immune responses through association with a transcriptional corepressor. Proc Natl Acad Sci U S A **107,** 13960-13965.

Zönnchen, J., Gantner, J., Lapin, D., Barthel, K., Eschen-Lippold, L., Erickson, J.L., Villanueva, S.L., Zantop, S., Kretschmer, C., Joosten, M.H.A.J., Parker, J.E., Guerois, R., and Stuttmann, J. (2022). EDS1 complexes are not required for PRR responses and execute TNL-ETI from the nucleus in Nicotiana benthamiana. New Phytol.

FIGURES LEGENDS

Figure 1: Membrane attachment is required for flax L6TIR signaling activity.

(A-D) Subcellular localization and (E-H) signaling activity (cell death/chlorosis) of yellow fluorescent protein (YFP) fusion of L6TIR and recombinants upon agro-mediated transient expression in flax leaves. Confocal images show YFP (yellow) labelling in Golgi bodies for L6TIR-YFP (A), in the nucleocytosol for P2/L6TIR-YFP (B), in the tonoplast for M/L6TIR-YFP (C) and mostly in the nucleocytosol for M*/L6TIR-YFP, overlayed with chloroplast autofluorescence (pink) and bright field images. Confocal images were taken 3 days after agro-infiltration (dai), in flax leaves. White bar scale represents 25µm. Photos of flax leaves (E-H) were taken 12dai. This experiment was repeated at least three times with similar results. (I) Immunoblot analysis of YFP fusion of L6TIR and recombinants upon agro-mediated transient expression in flax leaves. Samples were taken 3 days after agro-infiltration and detected with anti-GFP antibodies. Equal loading of proteins is indicated by red Ponceau staining

Figure 2: Fusion of signaling inactive P2/L6TIR to the flax rust effector AvrM leads to signaling activation in the cytosolic compartment only.

(A-B) Signaling activity of P2/L6 TIR-YFP and P2/L6 TIR-AvrM-YFP fusion series with a nuclear localization (NLS) or nuclear exclusion signal (NES) and corresponding mutants (nls and nes, respectively) upon agro-mediated transient expression in flax (A) or in *N. benthamiana* (B) leaves. Photos were taken 12 dai for flax and 5 dai for *N. benthamiana*. Infiltrated areas are surrounded by dotted circles (black dotted line circles correspond to positive controls). This experiment was repeated at least three times with similar results. (C) Ion leakage measurement of *N. benthamiana* leaves 48h after agro-mediated expression of mislocalized variants of P2/L6TIR fused to YFP or AvrM-YFP with a nuclear localization (NLS) or nuclear exclusion signal (NES) and corresponding mutants (nls and nes, respectively). Leaf disk samples were collected 2 days after infiltration and incubated in Milli-Q water. C1 corresponds to the ions released in solution 24 h after sampling (µs/cm). C2 corresponds to the total ion contents in the sample (µs/cm). Ion leakage was calculated as C1/C2 ratio (see methods for more details). *N. benthamiana* leaves infiltrated with empty agro strain (GV3103) were used as control. Statistical differences were calculated by one-way ANOVA followed by multiple comparison test (Tukey's HSD). Constructs sharing letters above boxplots are not significantly different ($\alpha = 0.05$, $n>8$). (D-E) Immunoblot analysis of mislocalized variants of P2/L6TIR fused to YFP or AvrM-YFP fusion series with a nuclear localization (NLS) or nuclear exclusion signal (NES) and corresponding mutants (nls and nes, respectively) upon transient

expression in flax (D) or *N. benthamiana* (E) leaves .Samples were taken 3 days or 48h after agro-infiltration in flax and *N. benthamiana*, respectively, and detected using anti-GFP antibodies. Equal loading of proteins is indicated by red Ponceau staining. Arrows point at the band size corresponding to P2/L6TIR fusion to AvrM-YFP (a), YFP (b) or to cleaved YFP (c).(F) Confocal images show YFP (yellow) labelling of mislocalized variants of P2/L6 TIR-YFP (left panel) or P2/L6 TIR-AvrM-YFP (right panel) constructs series fused to a nuclear localisation (NLS) or exclusion (NES) signal and corresponding mutants (nls and nes, respectively), overlayed with chloroplast autofluorescence (pink) and bright field images. Images were taken 48h after agroinfiltration in *N. benthamiana* leaves. White bar scale represents 25µm.

Figure 3: Forcing inactive RPS4TIR and SNC1TIR-only in the nucleus is sufficient to induce signaling.

(A-B) Signaling activity of YFP fusions of TIR-only SNC1 $^{1-179}$, RPS4 $^{1-193}$ and P2/L6TIR (left part of the leaf) and signaling active SNC1 $^{1-226}$, RPS4 $^{1-235}$ and L6TIR, upon agro-mediated transient expression in leaves of *N. benthamiana* (A) and *N. tabacum* (B). (C) Immunoblot analysis of TIR-only (RPS4 $^{1-193}$ and SNC1 $^{1-179}$) or larger TIR constructs (RPS4 $^{1-235}$ and SNC1 $^{1-226}$) upon transient expression in *N. benthamiana* leaves. Samples were taken 48h after agro-infiltration and detected with anti-GFP antibodies. Equal loading of proteins is indicated by red Ponceau staining. (D-G) Signaling activity of mislocalized variants of RPS4 $^{1-193}$ and SNC1 $^{1-179}$ fused to YFP (D,F) or AvrM-YFP (E,G) with a nuclear localization (NLS) or nuclear exclusion signal (NES) and corresponding mutants (nls and nes, respectively) upon agro-mediated transient expression in *N. benthamiana.* Photos were taken 5 dai. Infiltrated areas are surrounded by dotted circles (black dotted line circles correspond to positive controls). These experiments were repeated at least three times with similar results. (H-I) Ion leakage measurement of *N. benthamiana* leaves 48h after agro-mediated expression of mislocalized variants of RPS4 $^{1-193}$ (H) or SNC1 $^{1-179}$ (I) fused to YFP or AvrM-YFP with a nuclear localization (NLS) or nuclear exclusion signal (NES) and corresponding mutants (nls and nes, respectively). Leaf disk samples were collected 2 days after infiltration and incubated in Milli-Q water. C1 corresponds to the ions released in solution 24 h after sampling. C2 corresponds to the total ion contents in the sample. Ion leakage was calculated as C1/C2 ratio (see methods for more details). *N. benthamiana* leaves infiltrated with signaling active RPS4 $^{1-235}$ or SNC1 $^{1-226}$ were used as positive controls, respectively. Statistical differences was calculated by one-way ANOVA followed by multiple comparison test (Tukey's HSD). Constructs sharing letters above boxplots are not significantly different ($\alpha = 0.05$, n=4 for RPS4TIR serie, n>8 for SNC1TIR serie). (J-K) Immunoblot analysis of RPS4 $^{1-193}$ and SNC1 $^{1-179}$ fused to YFP or AvrM-YFP with a nuclear localization (NLS) or nuclear exclusion signal (NES) and corresponding mutants (nls and nes, respectively) upon

transient expression in *N. benthamiana* leaves. Samples were taken 48h after agro-infiltration and detected with anti-GFP antibodies. Equal loading of proteins is indicated by red Ponceau staining.

Figure 4: Altered subcellular localization of signaling active RPS4 and SNC1 TIR domains do not affect their ability to induce immune responses.

(A-B) Signaling activity of mislocalized variants of RPS4 $^{1-235}$ and SNC1 $^{1-226}$ fused to YFP with a nuclear localization (NLS) or nuclear exclusion signal (NES) and corresponding mutants (nls and nes, respectively) upon agro-mediated transient expression in *N. benthamiana.* (C-D) Immunoblot analyses of RPS4 $^{1-235}$ (C) and SNC1 $^{1-226}$ (D) fused to YFP with a nuclear localization (NLS) or nuclear exclusion signal (NES) and corresponding mutants (nls and nes, respectively) upon transient expression in *N. benthamiana* leaves. Samples were taken 48h after agroinfiltration. Proteins were detected with anti-GFP antibodies. Equal loading of proteins is indicated by red Ponceau staining. (E-F) Signaling activity of RPS4 $^{1-235}$-YFP and SNC1TIR $^{1-226}$-YFP fused to the flax L6 Golgi membrane signal anchor in their N-terminus, upon agro-mediated transient expression at OD_{600}=0,1 in *N.benthamiana*. (E) Photos of cell death symptoms were taken 5 dai. Infiltrated areas are surrounded by dotted circles (black dotted line circles correspond to positive controls). These experiments were repeated at least three times with similar results. (F) Ion leakage measurement of *N. benthamiana* leaves 48h after agro-mediated expression of mislocalized variants of RPS4 $^{1-235}$ and SNC1 $^{1-226}$ fused to YFP. Leaf disk samples were collected 2 days after infiltration and incubated in Milli-Q water. C1 corresponds to the ions released in solution 24 h after sampling (µs/cm). C2 corresponds to the total ion contents in the sample (µs/cm). Ion leakage was calculated as C1/C2 ratio (see methods for more details). Statistical differences were calculated by one-way ANOVA followed by multiple comparison test (Tukey's HSD). Constructs sharing letters above boxplots are not significantly different ($\alpha = 0.05$, $n>6$).

Figure 5: Subcellular requirement of AtEDS1 for flax L6 signaling in Arabidopsis.

(A) Signaling activity of flax L6 in transgenic Arabidopsis seedlings (10 day-old) expressing Dexamethasone (Dex)-inducible L6 MHV autoimmune variant in *eds1-2* mutant background complemented with mislocalized EDS1-YFP variants. F3 individuals from each cross (pDex:L6MHV-3myc x *eds1-2) x* pEDS1:EDS1-YFP mislocalized variants (pEDS1:EDS1-YFP-NLS (#B2) pEDS1:EDS1-YFP-NES (#3-4), pEDS1:EDS1-YFP-nls (#B5), pEDS1:EDS1-YFP-nes (#1-2)) were PCR screened to verify the presence or absence (-) of EDS1-YFP variant transgene and transferred to 10µM Dex-containing media. Photos were taken on the day plants were transferred (t0), and four (4dai) and eight (8dai) days after transfer (dai:days after Dex induction). Transgenic pDex:L6MHV-3myc and wild-type Col-0 seedlings were used as positive and negative controls,

respectively. This assay was repeated three times with similar results. (B) Immunoblot analysis of EDS1-YFP variants and L6MHV-3myc 24h after Dex induction, using anti-GFP and anti-myc antibodies, respectively. Protein loading is indicated by red Ponceau staining.

Figure 6: Subcellular requirement of AtEDS1 for flax RPS4TIR signaling in Arabidopsis.
(A) Signaling activity of Arabidopsis RPS4 TIR in transgenic Arabidopsis seedlings (10 day-old) expressing Dexamethasone (Dex)-inducible RPS4 $^{1-235}$ in *eds1-2* mutant background complemented with mislocalized EDS1-YFP variants. F3 individuals from each cross (pDex: RPS4 $^{1-235}$ -Flag-SBP x *eds1-2) x* pEDS1:EDS1-YFP mislocalized variants (pEDS1:EDS1-YFP-NLS (#B2) pEDS1:EDS1-YFP-NES (#3-4), pEDS1:EDS1-YFP-nls (#B5), pEDS1:EDS1-YFP-nes (#1-2)) were PCR screened to verify the presence or absence of EDS1-YFP variant transgene and transferred to 10µM Dex-containing media. Photos were taken on the day plants were transferred (t0), three (3dai) and six (6dai) days after transfer (dai:days after Dex induction). Transgenic pDex: RPS4 $^{1-235}$-FSBP and wild-type Col-0 seedlings were used as positive and negative controls, respectively. This assay was performed twice with similar results. pDex:EDS1-YFP-NES (line#2) is a sibling line of pDex:EDS1-YFP-NES (line#1) but in which the EDS1-YFP-NES transgene is homozygous unlike line#1 in which the transgene still segregates. (B) Immunoblot analysis of EDS1-YFP variants and RPS4 $^{1-235}$ -flag-SBP 24h after Dex induction, using anti-GFP and anti-flag antibodies, respectively. Protein loading is indicated by red Ponceau staining.

Figure 1: Membrane attachment is required for flax L6TIR signaling activity

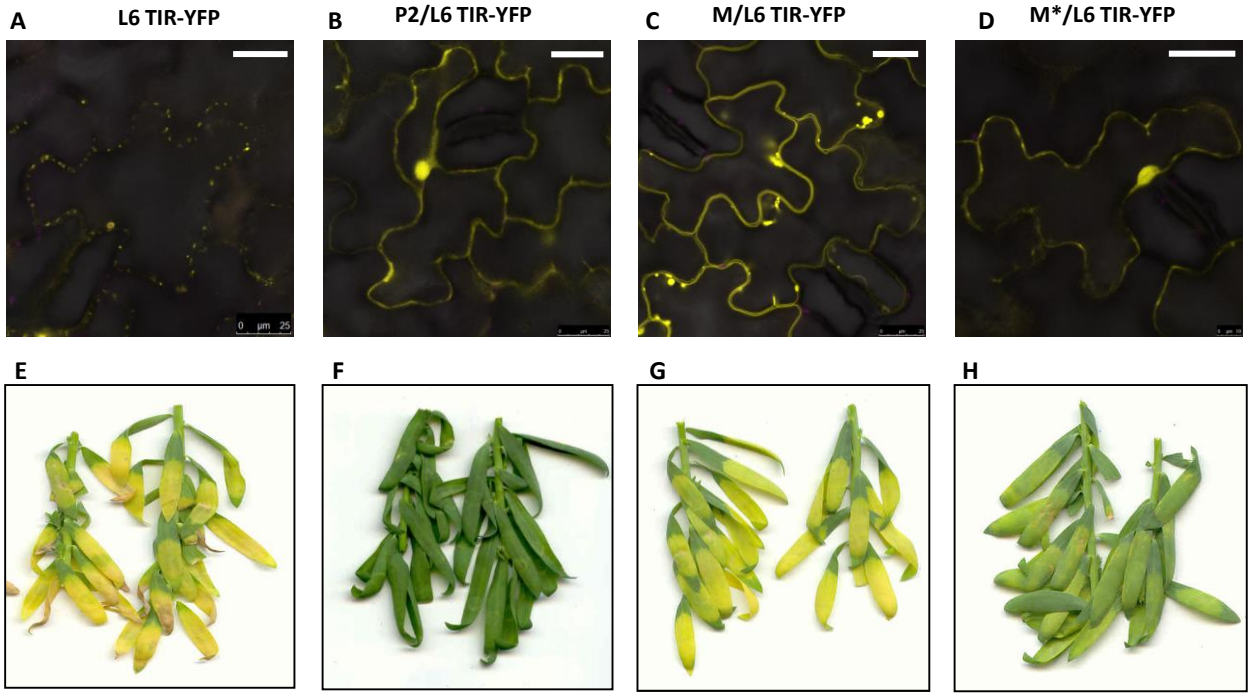

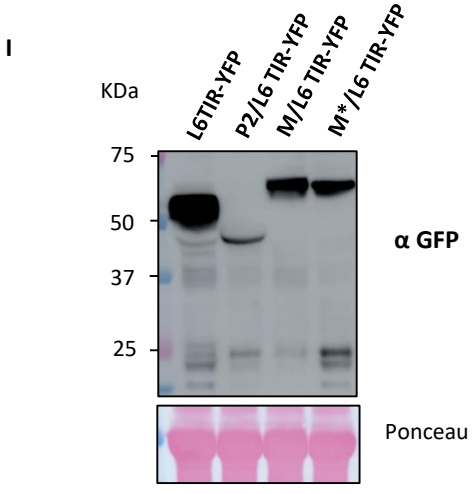

Figure 2: Fusion of signaling inactive P2/L6TIR to the flax rust effector AvrM leads to TIR signaling activation in the cytosolic compartment only

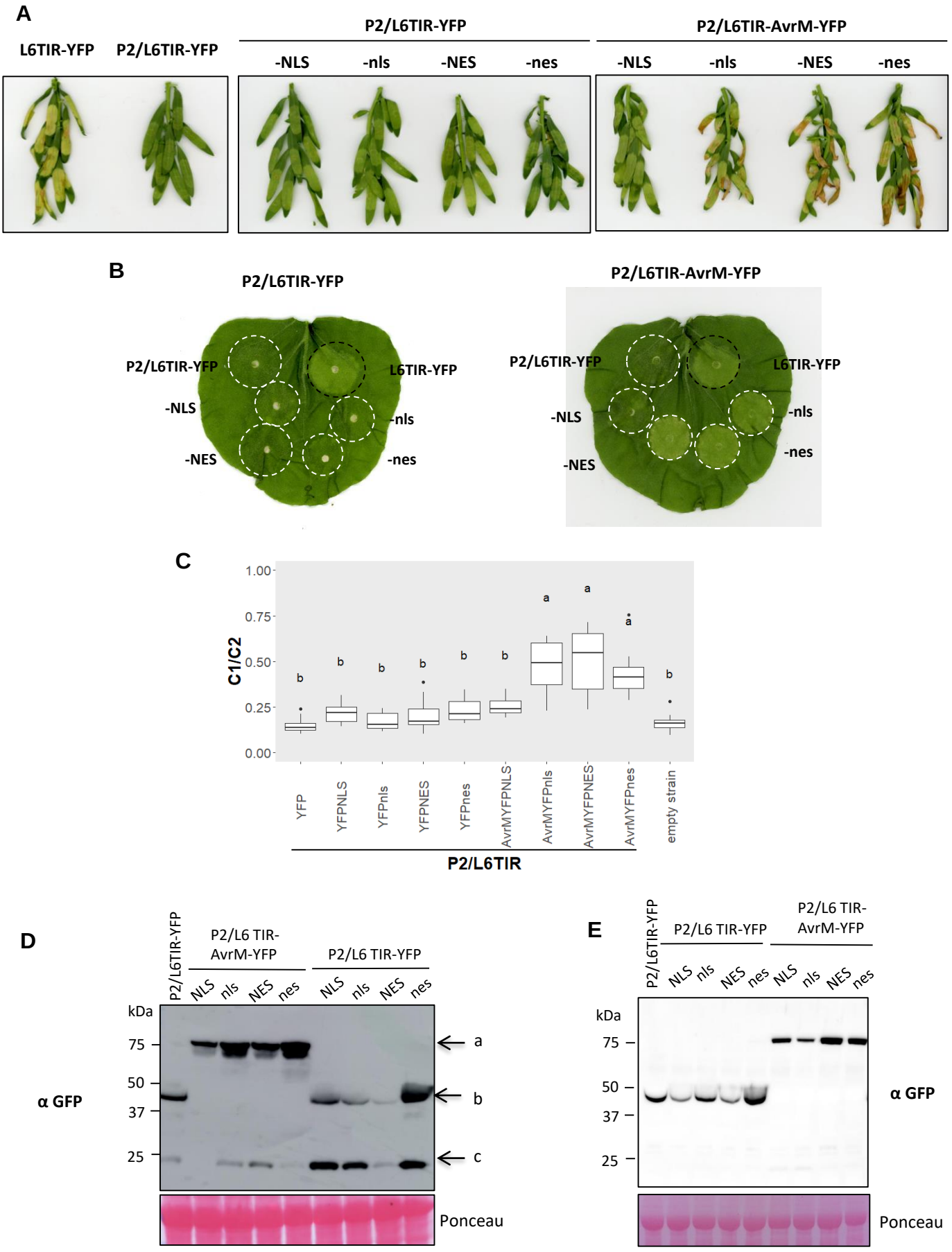

F

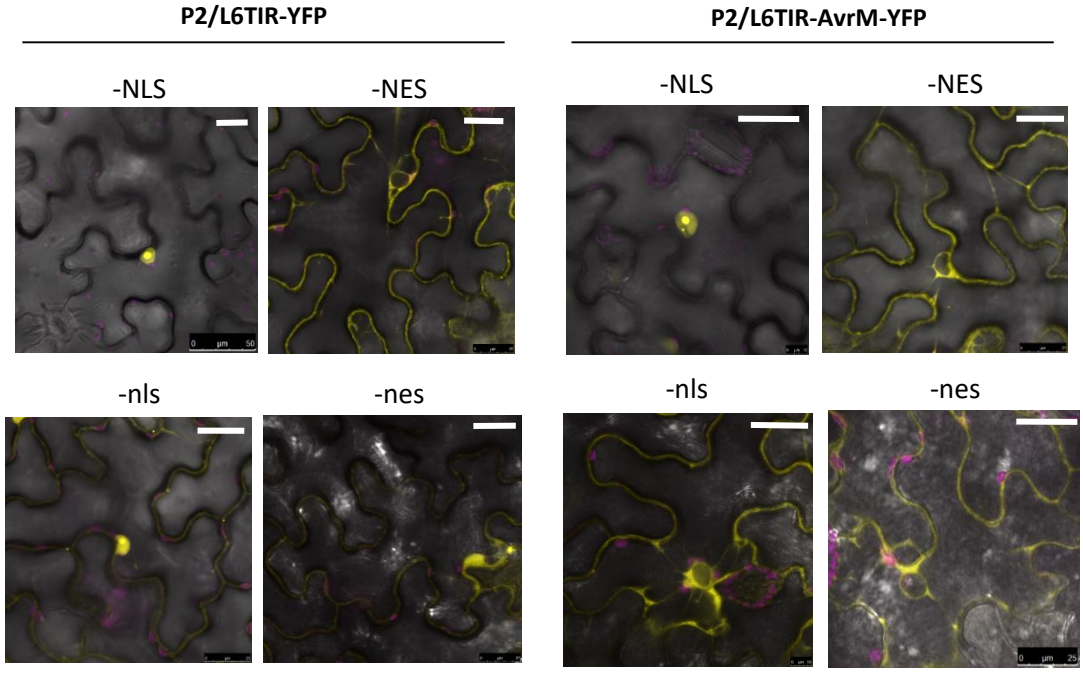

Figure 3: Forcing inactive RPS4TIR and SNC1TIR-only in the nucleus is sufficient to activate TIR signaling

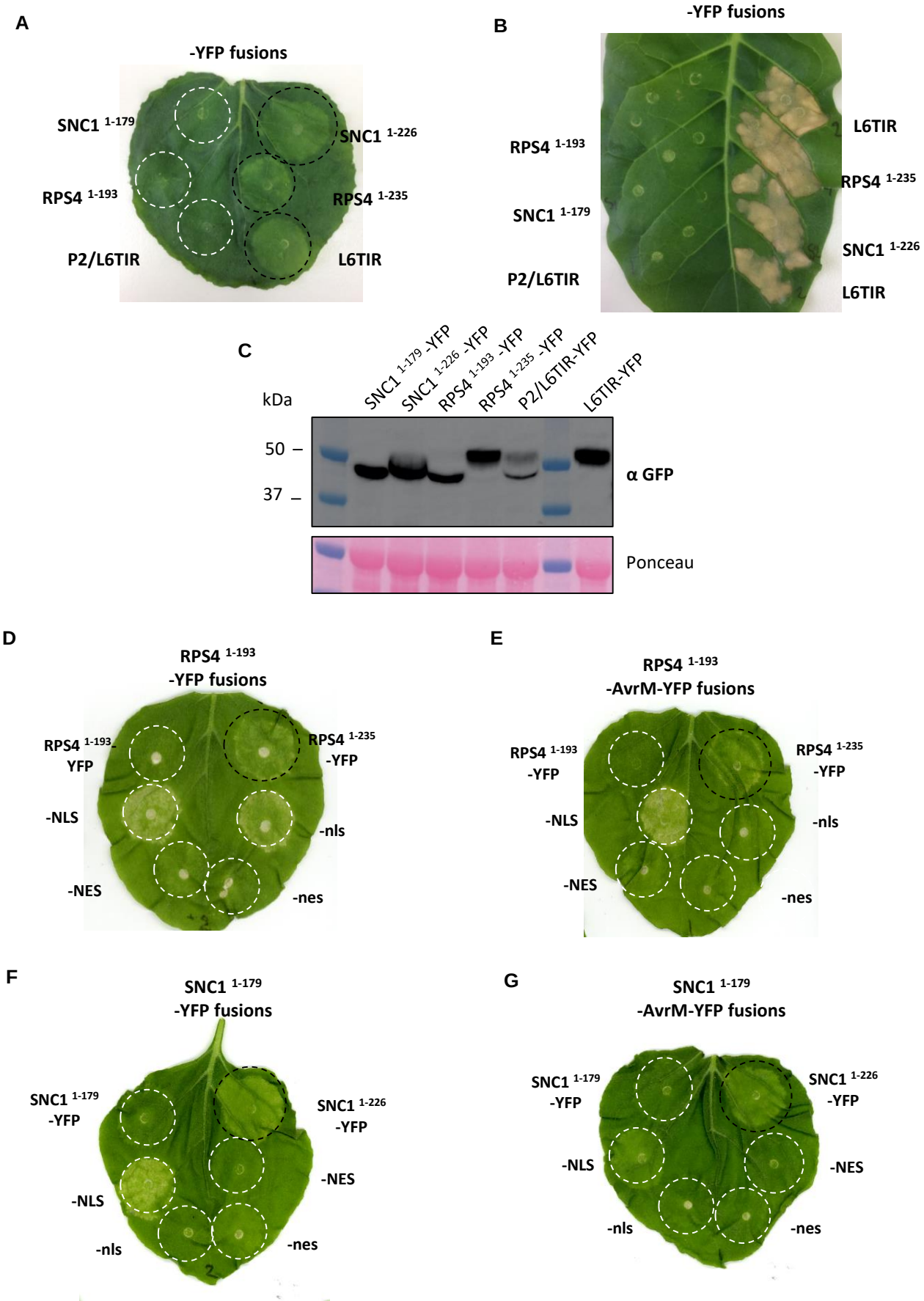

H

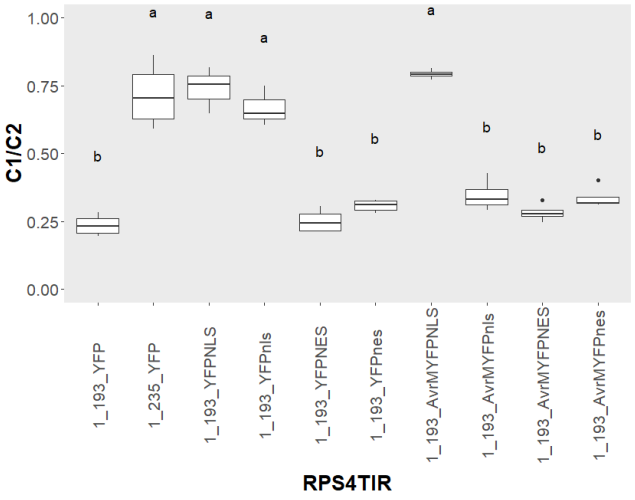
C1/C2
1.00
0.75
0.50
0.25
0.00
a
a
a
b
b
b
a
b
b
b
1_193_YFP
1_235_YFP
1_193_YFPNLS
1_193_YFPnls
1_193_YFPNES
1_193_YFPnes
1_193_AvrMYFPNLS
1_193_AvrMYFPnls
1_193_AvrMYFPNES
1_193_AvrMYFPnes
RPS4TIR

I

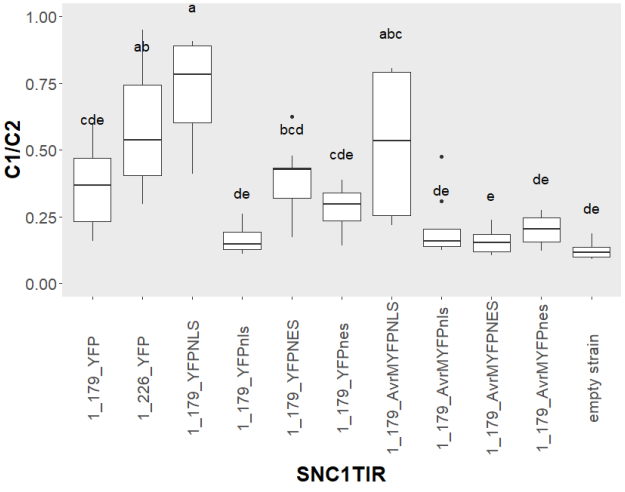
C1/C2
1.00
0.75
0.50
0.25
0.00
cde
ab
a
de
bcd
cde
abc
de
e
de
de
1_179_YFP
1_226_YFP
1_179_YFPNLS
1_179_YFPnls
1_179_YFPNES
1_179_YFPnes
1_179_AvrMYFPNLS
1_179_AvrMYFPnls
1_179_AvrMYFPNES
1_179_AvrMYFPnes
empty strain
SNC1TIR

J

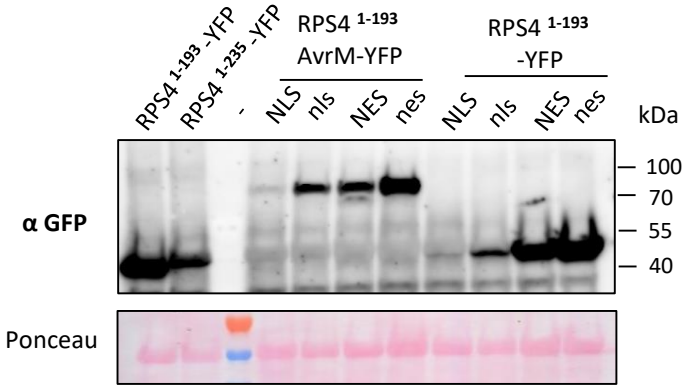
RPS4 1-193 -YFP
RPS4 1-235 -YFP
-
RPS4 1-193 AvrM-YFP
NLS
nls
NES
nes
RPS4 1-193 -YFP
NLS
nls
NES
nes
kDa
100
70
55
40
α GFP
Ponceau

K

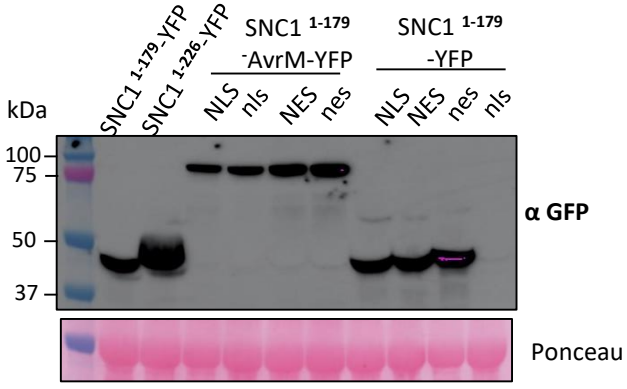
kDa
SNC1 1-179 -YFP
SNC1 1-226 -YFP
SNC1 1-179 -AvrM-YFP
NLS
nls
NES
nes
SNC1 1-179 -YFP
NLS
NES
nes
nls
100
75
50
37
α GFP
Ponceau

Figure 4: Altered subcellular localization of signaling active RPS4 and SNC1 TIR domains do not affect their ability to induce immune responses

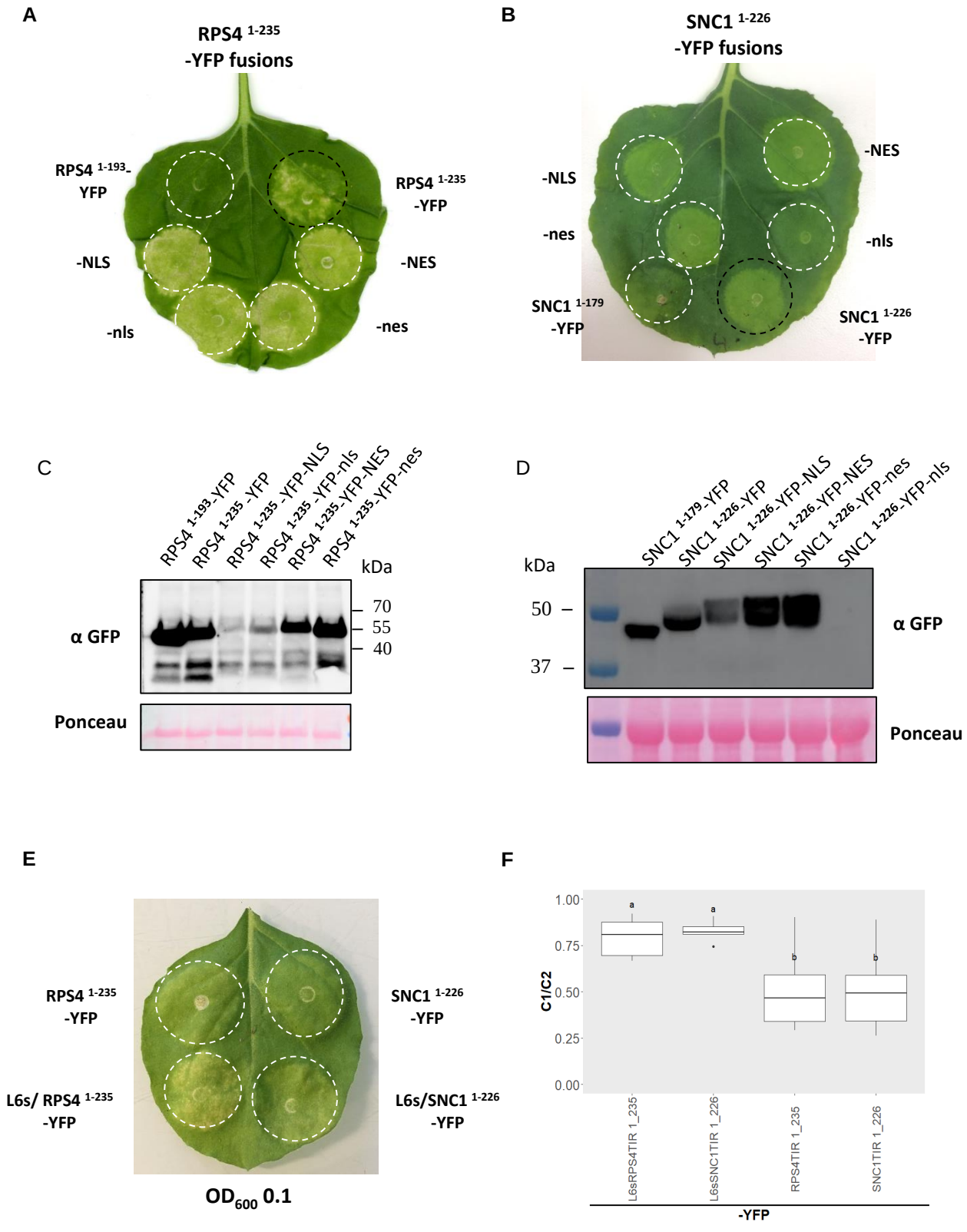

Figure 5: Subcellular requirement of AtEDS1 for flax L6 signaling in Arabidopsis

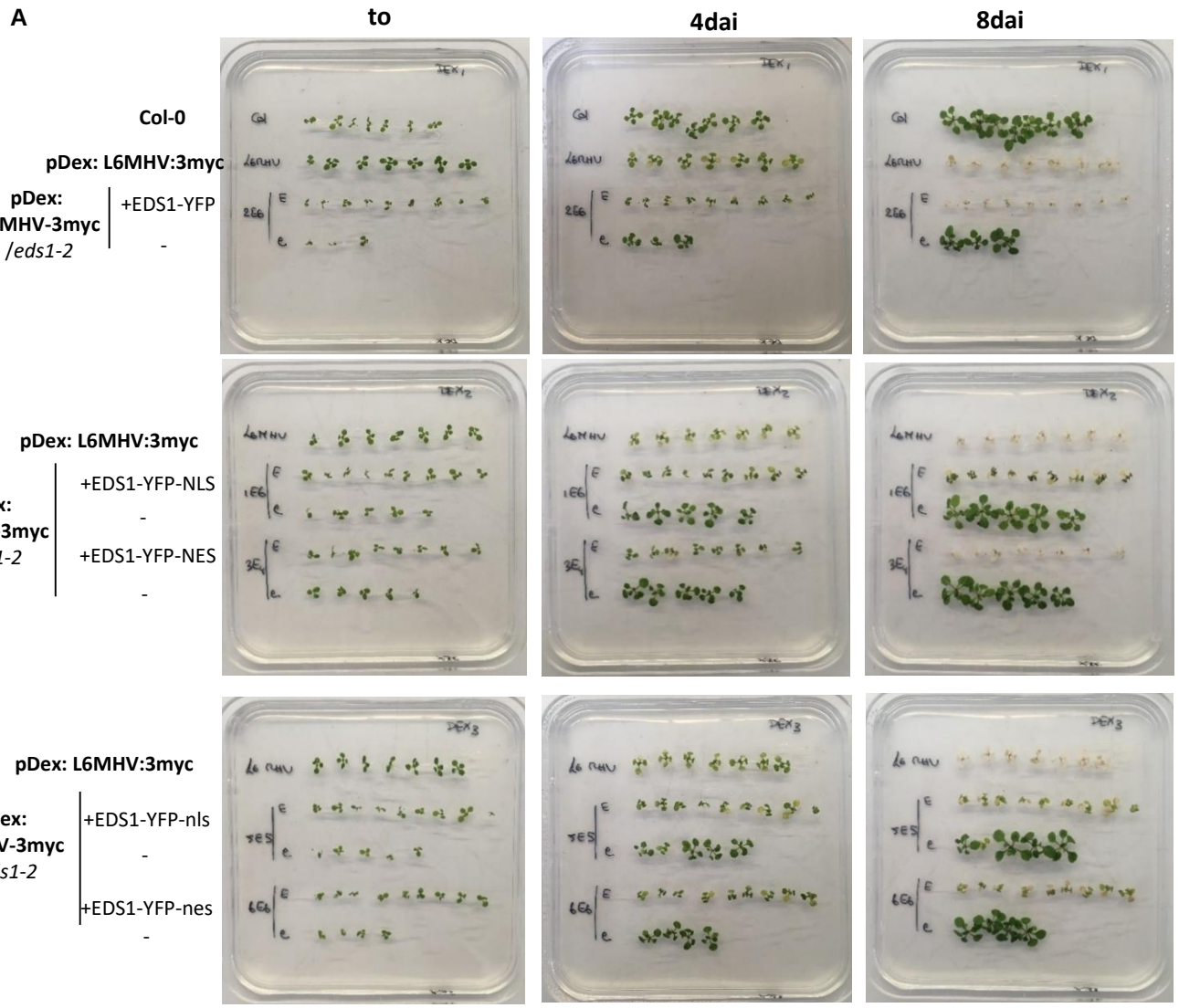

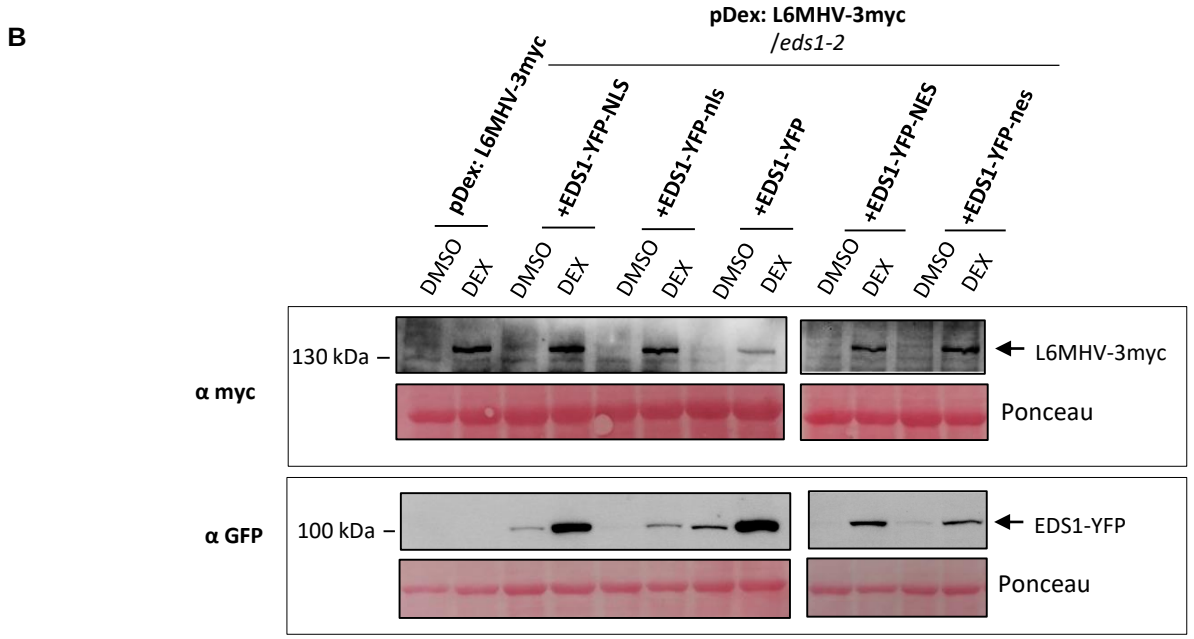

Figure 6: Subcellular requirement of AtEDS1 for flax RPS4TIR signaling in Arabidopsis

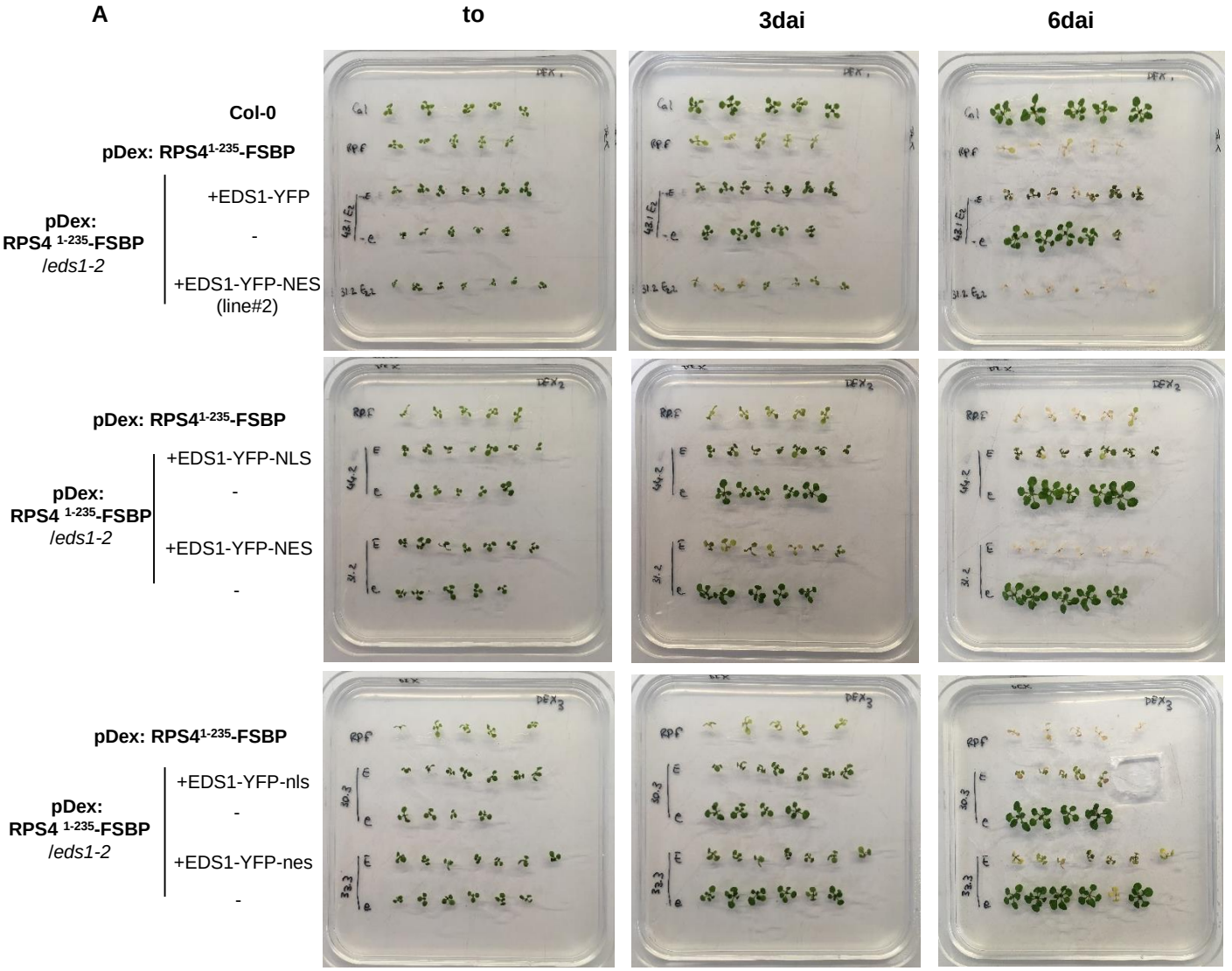

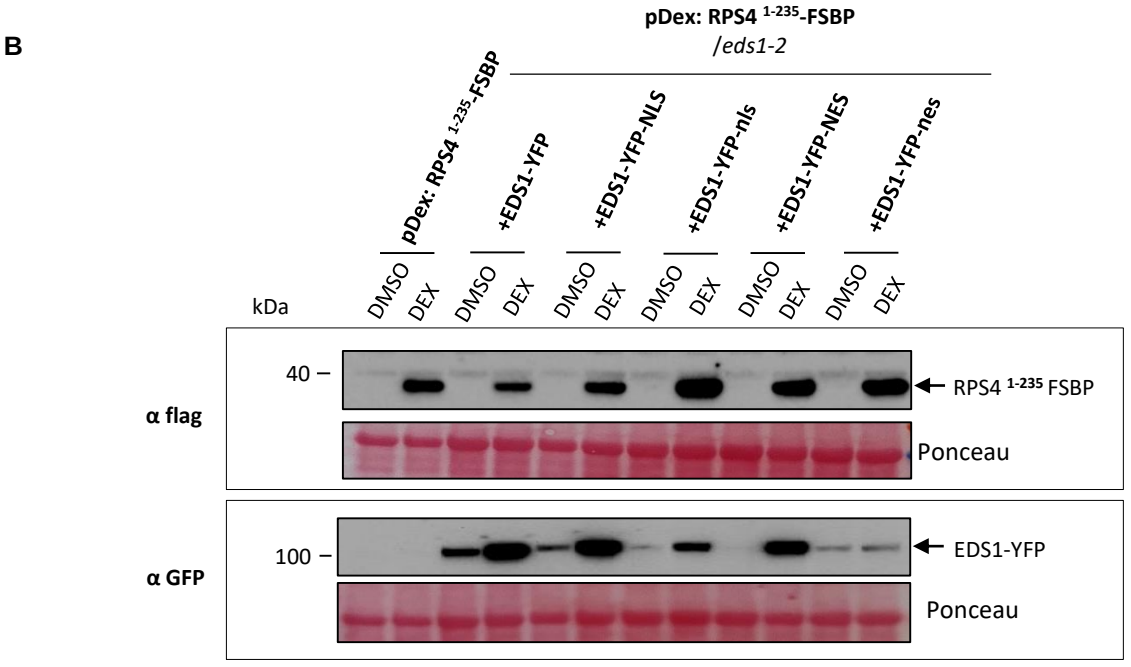

Supplemental figures

Figure S1: Signalling activity, and protein stability of mislocalized variants of P2/L6TIR.
(A) Signaling activity of L6TIR and P2/L6 TIR fused to -YFP or flax rust effector –AvrM upon agro-mediated transient expression in flax . Photos were taken 12 dai. (B) Live cell fluorescence image show YFP (yellow) cytosolic labelling of AvrM-YFP, overlayed with chloroplast autofluorescence (pink). Confocal images were taken 48h after agro-infiltration, in *N. benthamiana* leaves. White bar scale represents 25µm.

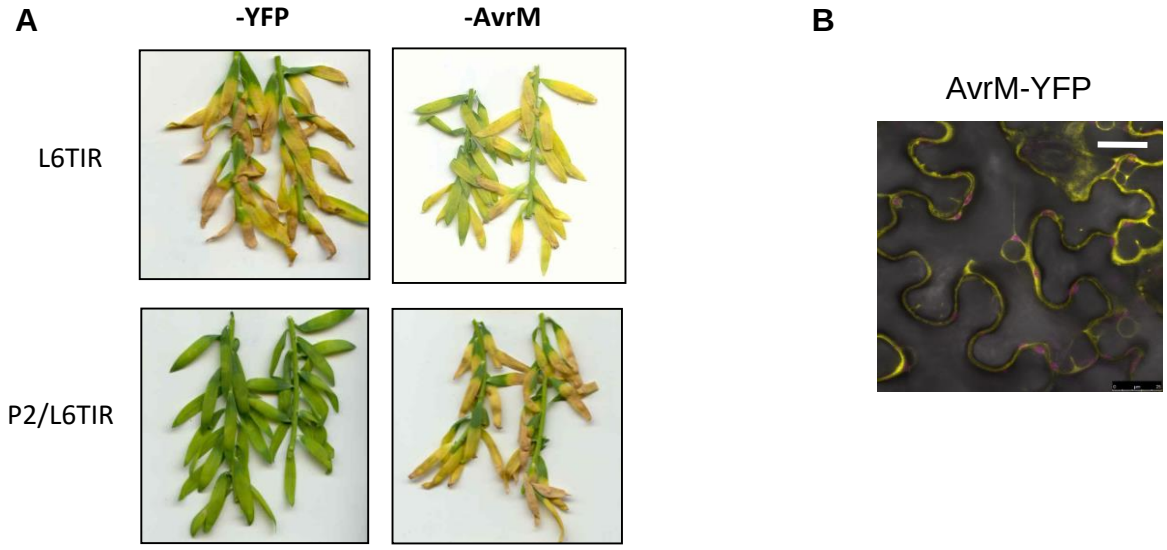

Figure S2: Signalling activity of membrane-tethered L6 TIR is not affected by a fusion to AvrM and a nuclear localization or nuclear exclusion signal.

(A) Signaling activity of L6 TIR-YFP and L6 TIR-AvrM-YFP fusion series with a nuclear localization (NLS) or nuclear exclusion signal (NES) and corresponding mutants (nls and nes, respectively) upon agro-mediated transient expression in flax . Photos were taken 12 dai. (B) Live cell fluorescence images show YFP (yellow) labelling of mislocalized variants of L6 TIR-YFP or L6 TIR-AvrM-YFP constructs series fused to a nuclear localisation (NLS) or exclusion (NES) signal, overlayed with chloroplast autofluorescence (pink). Confocal images were taken 48h after agro-infiltration, in *N. benthamiana* leaves. White bar scale represents 25µm. (C) Immunoblot analysis of mislocalized variants of P2/L6TIR fused to YFP or AvrM-YFP fusion series with a nuclear localization (NLS) or nuclear exclusion signal (NES) and corresponding mutants (nls and nes, respectively) upon transient expression in *N. benthamiana* leaves. Samples were taken 48h after agro-infiltration and detected with anti-GFP antibodies. Equal loading of proteins is indicated by red Ponceau staining.

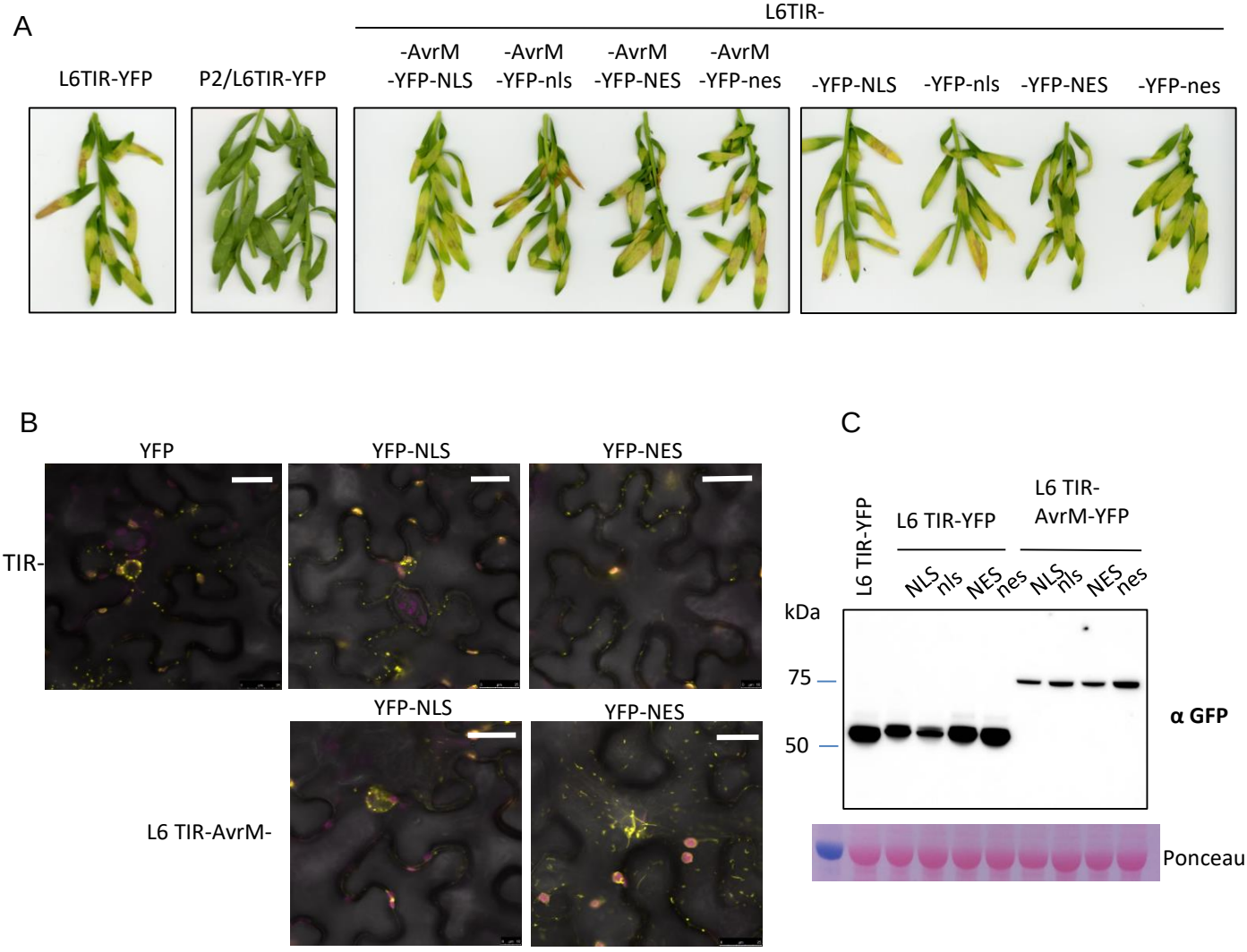

Figure S3: Subcellular localization of RPS4 and SNC1 TIR constructs.
Live cell fluorescence images show YFP (yellow) labelling of TIR-only (RPS4 $^{1-193}$ and SNC1 $^{1-179}$) or larger TIR constructs (RPS4 $^{1-235}$ and SNC1 $^{1-226}$), overlayed with chloroplast autofluorescence (pink). Confocal images were taken 48h after agro-infiltration, in *N. benthamiana* leaves. White bar scale represents 25µm.

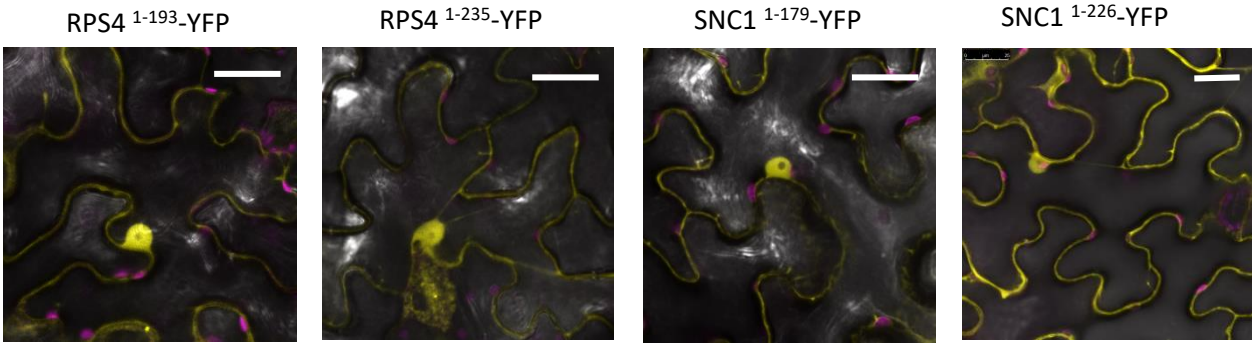

Figure S4: **Subcellular localization of mislocalized variants of RPS4 and SNC1 TIR-only.**
Live cell fluorescence images show YFP (yellow) labelling of RPS4 $^{1-193}$ (A) and SNC1 $^{1-179}$ (B) fused to YFP or AvrM-YFP with a nuclear localization (NLS) or nuclear exclusion signal (NES) and corresponding mutants (nls and nes, respectively), overlayed with chloroplast autofluorescence (pink). Confocal images were taken 48h after agro-infiltration, in *N. benthamiana* leaves. White bar scale represents 25µm.

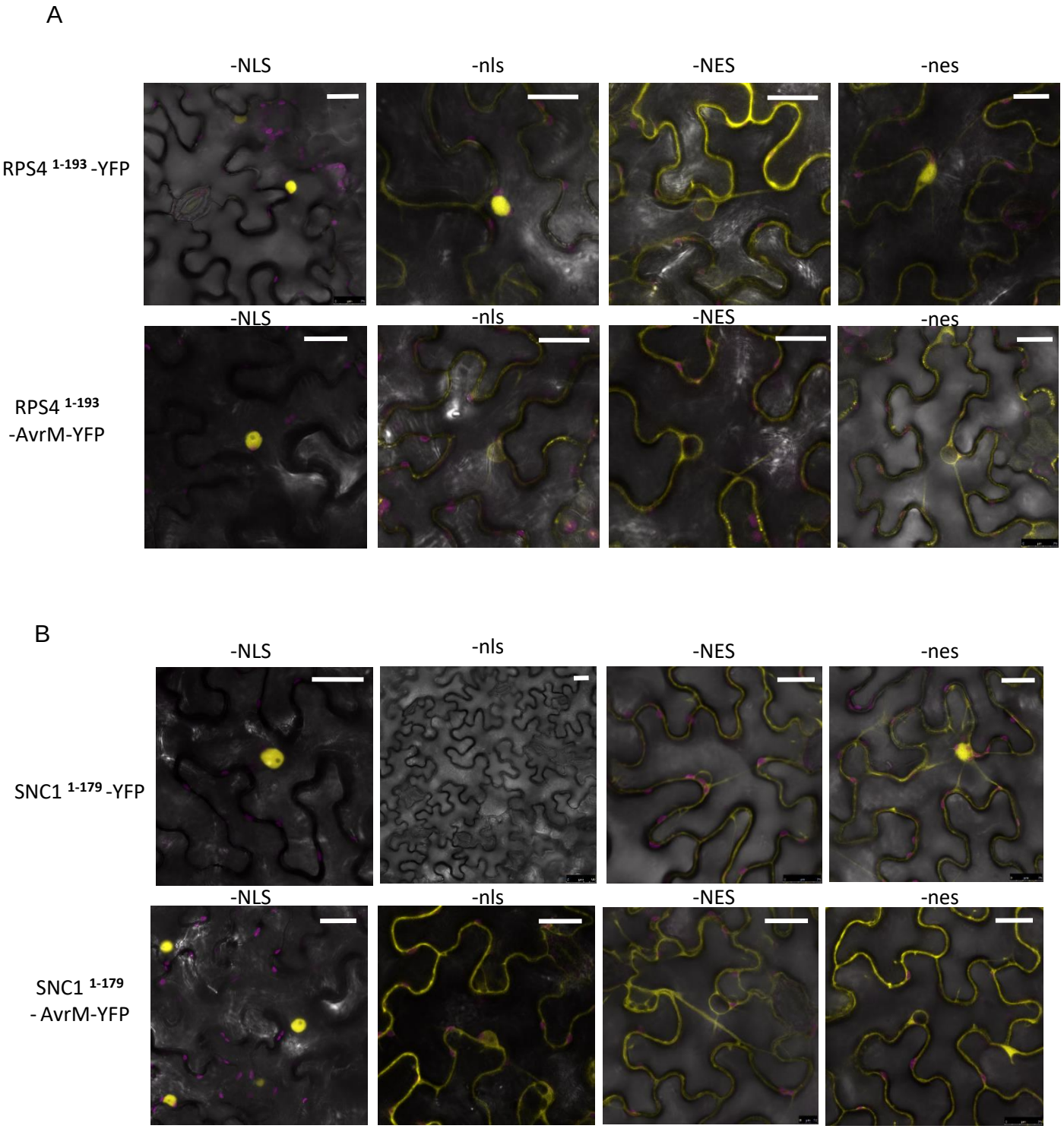

Figure S5: S**ubcellular localization of mislocalized variants of RPS4 $^{1-235}$ and SNC1 $^{1-226}$ TIR constructs.**
Immunoblot (A) and confocal analyses (B) of RPS4 $^{1-235}$ and SNC1 $^{1-226}$ fused to YFP with a nuclear localization (NLS) or nuclear exclusion signal (NES) and corresponding mutants (nls and nes, respectively) upon transient expression in *N. benthamiana* leaves. (A) Samples were taken 48h after agroinfiltration. Proteins were detected with anti-GFP antibodies. Equal loading of proteins is indicated by red Ponceau staining. (B) Live cell fluorescence images show YFP (yellow) labelling overlayed with chloroplast autofluorescence (pink). Confocal images were taken 48h after agro-infiltration, in *N. benthamiana* leaves. White bar scale represents 25µm.

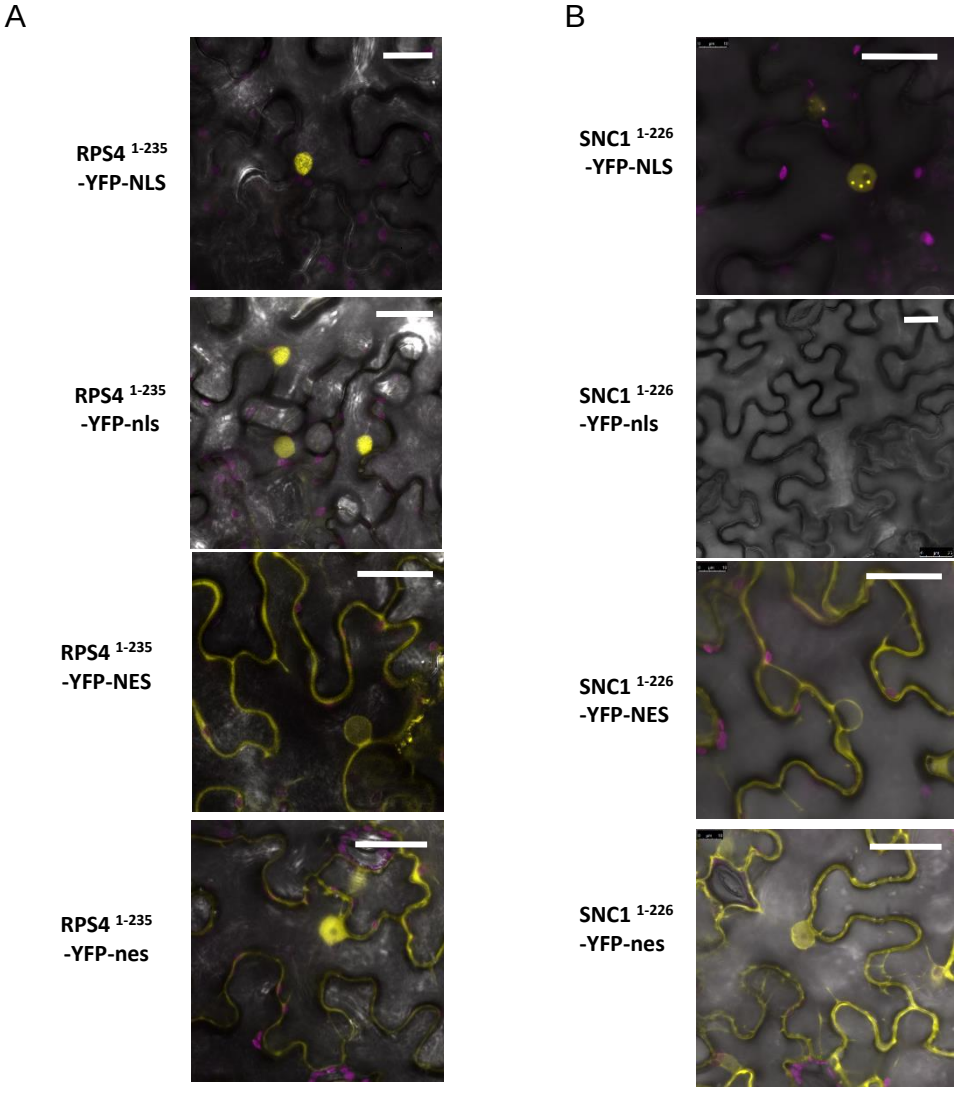

Figure S6: **Signaling activity, subcellular localization and protein accumulation of RPS4 $^{1-235}$ and SNC1 $^{1-226}$ TIR constructs fused to L6 signal anchor. (See legends next slide)**

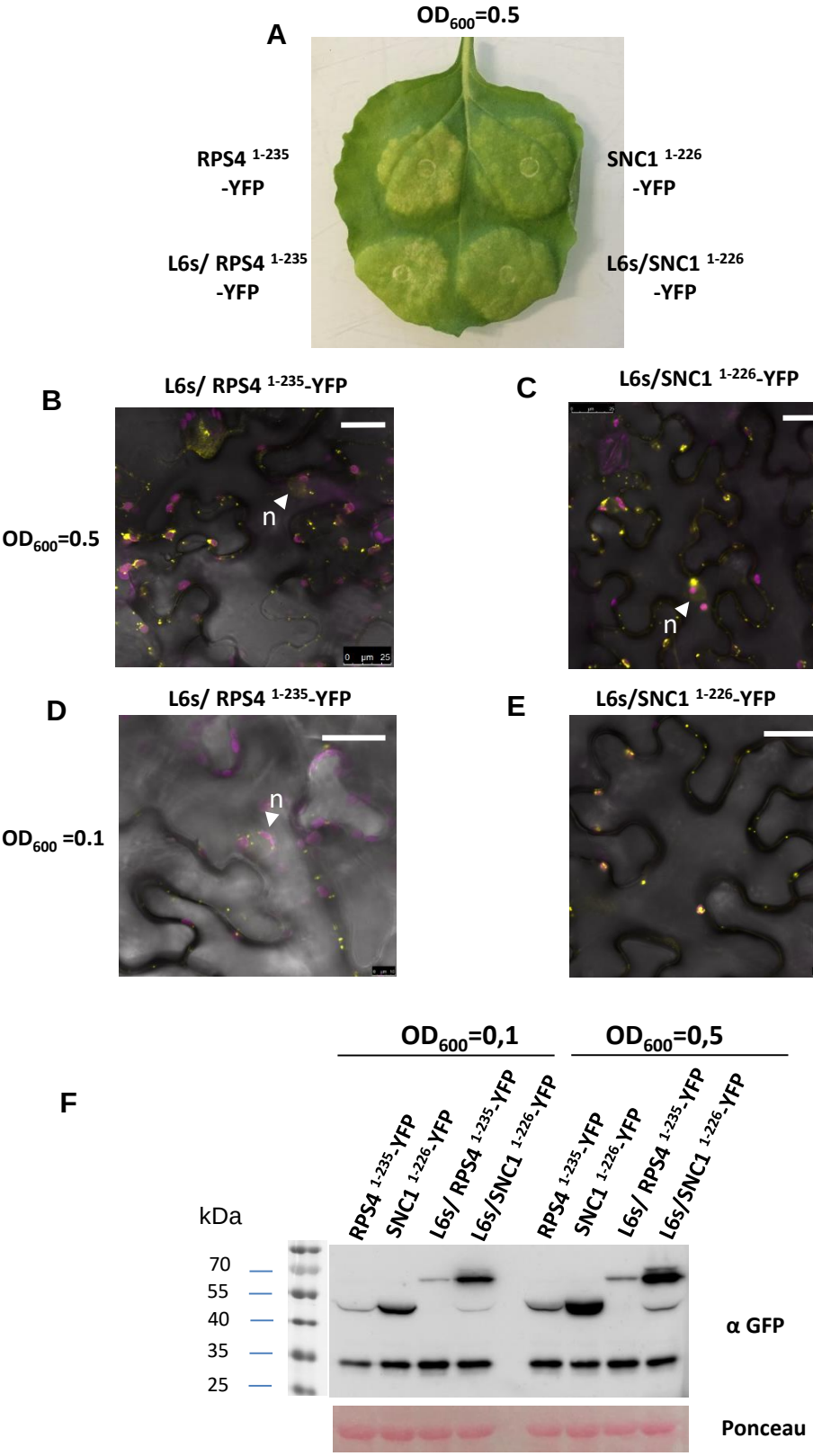

Figure S6: **Signaling activity, subcellular localization and protein accumulation of RPS4 $^{1-235}$ and SNC1 $^{1-226}$ TIR constructs fused to L6 signal anchor.**

Signalling activity (A), subcellular localization (B-E) and protein accumulation (F) of RPS4 $^{1-235}$ and SNC1 $^{1-226}$ TIR constructs fused to L6 signal anchor upon transient expression in *N. benthamiana*.

(A) N. *bentamiana* leaves photos were taken 5 days after agro-infiltration at OD_{600} 0.5 in *N. benthamiana*. (B-E) Live cell fluorescence images show YFP (yellow) labelling of Golgi membrane-tethered RPS4 $^{1-235}$ and SNC1 $^{1-226}$ TIR constructs fused to L6 signal anchor, overlayed with chloroplast autofluorescence (pink). Confocal images were taken 48h after agro-infiltration at OD_{600} 0.5 or OD_{600} 0.1, in *N. benthamiana* leaves. The arrow head points at a nucleus (n). White bar scale represents 25µm. (F) Immunoblot analysis. Proteins were detected using anti-GFP antibodies. Equal loading of proteins is indicated by red Ponceau staining.

Figure S7: Phenotype of independent transgenic Arabidopsis seedlings expressing Dexamethasone (Dex)-inducible L6MHV-3myc (pDex:L6MHV-3myc).
F2 individuals (10 day-old) were transferred to non-inducing (DMSO) or 10µM Dex-containing media. Photos were taken 14 days after transfer.

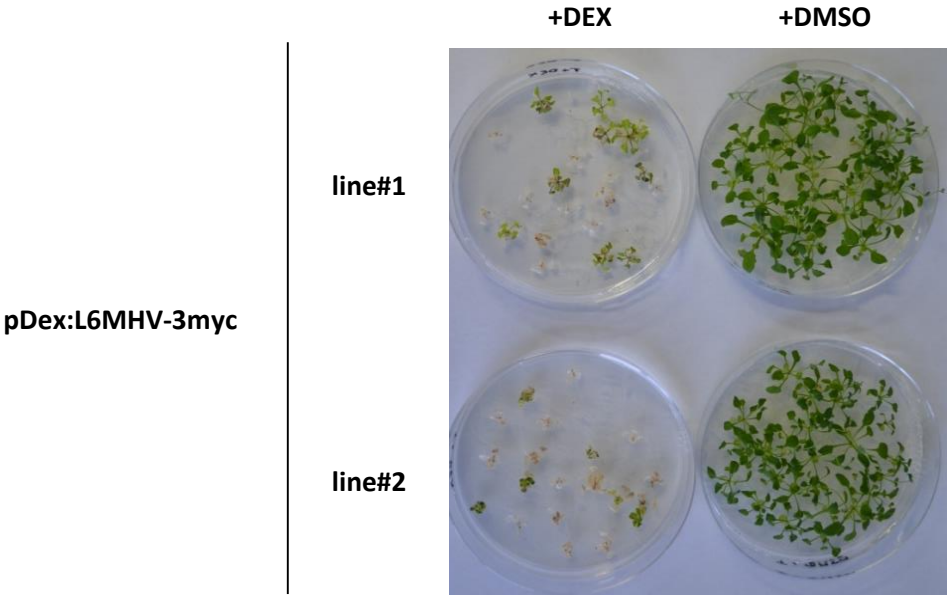

Figure S8: Phenotype of transgenic Arabidopsis seedlings expressing pDex:L6MHV on a non-inducing media.

F3 individuals of transgenic Arabidopsis seedlings (10 day-old) expressing Dexamethasone (Dex)-inducible L6MHV-3myc in wild-type Col-0 or in *eds1-2* mutant background complemented with mislocalized EDS1-YFP variants (pDex:L6MHV-3myc x *eds1-2) x* pEDS1:EDS1-YFP mislocalized variants. Each individuals were PCR screened to verify the presence or absence of EDS1-YFP variant transgene and transferred to non-inducing (DMSO containing) MS media. Photos were taken on the day plants were transferred (t0) , four (3dai) and eight (6dai) days after transfer (dai: days after induction). This assay was performed two times with similar results.

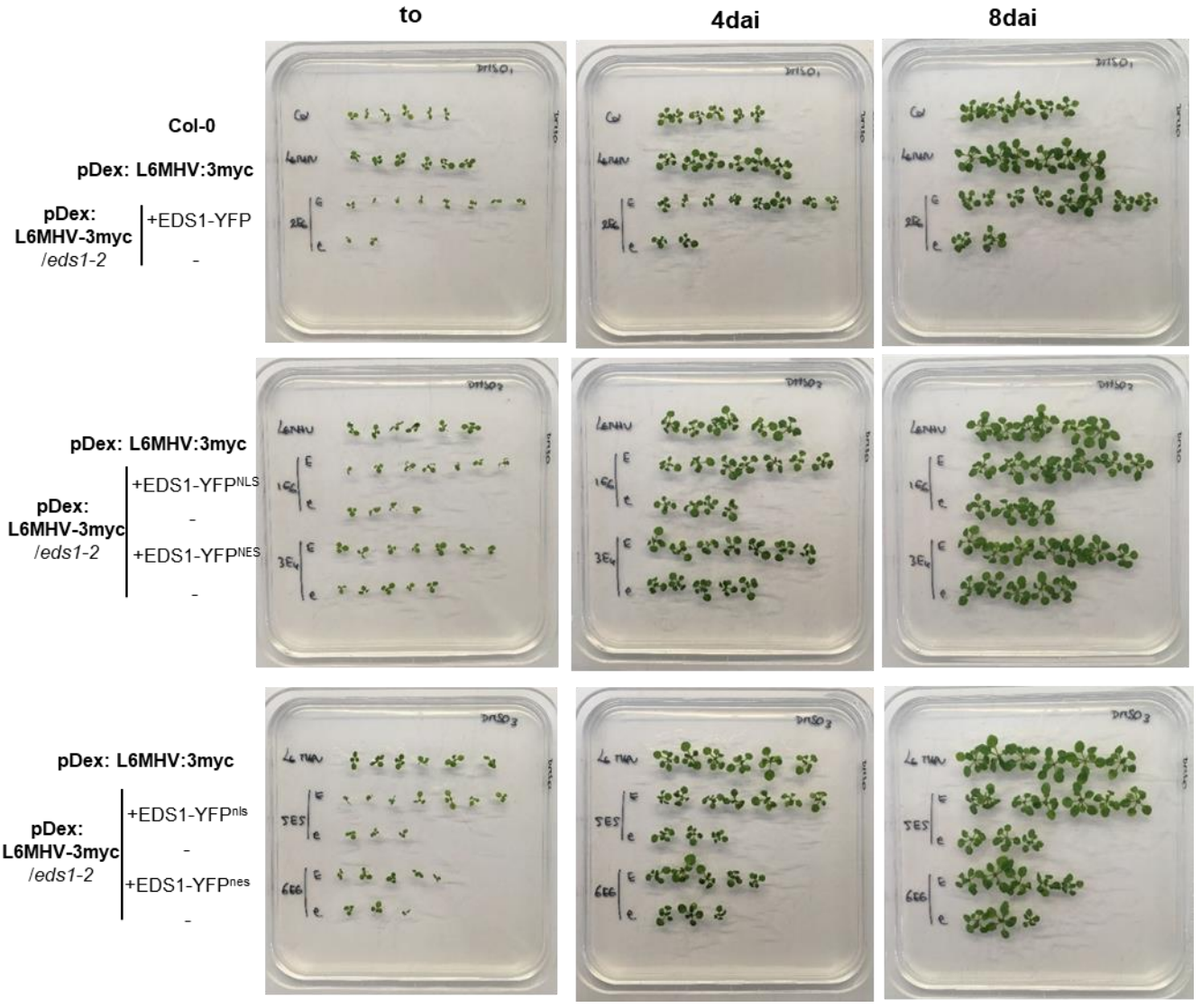

Figure S9: Flax L6 signaling in Arabidopsis depends on AtEDS1.
Cell death phenotype of transgenic Arabidopsis seedlings (10 day-old) expressing Dexamethasone (Dex)-inducible L6MHV-3myc in *eds1-2* mutant background. F2 individuals from pDex:L6MHV-3myc x *eds1-2* (line #2) were PCR screened to select seedlings homozygous for *EDS1* mutation (*eds1/eds1*) or displaying heterozygous or homozygous wild-type *EDS1 (EDS1/eds1 or EDS1/EDS1).* Seedlings were transferred to 10µM Dex-containing media. Photos were taken 6 days after Dex induction.

Col-0

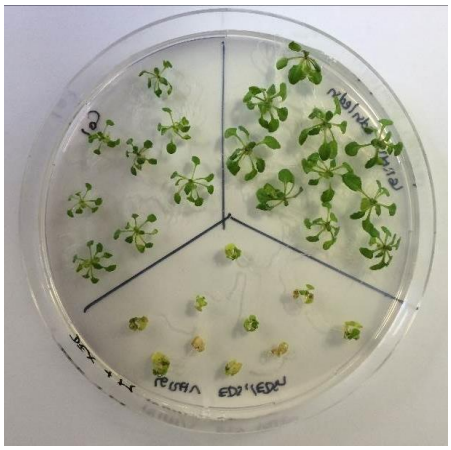

pDex:L6MHV-3myc
X *eds1-2*
(eds1/eds1)

pDex:L6MHV-3myc
X *eds1-2*
(*EDS1/EDS1* or *EDS1/eds1)*

Figure S10: Phenotype of transgenic Arabidopsis seedlings from crosses of pDex:L6MHV-3myc/*eds1-2* line with independent mislocalized EDS1 variants lines. (See legends next slide).

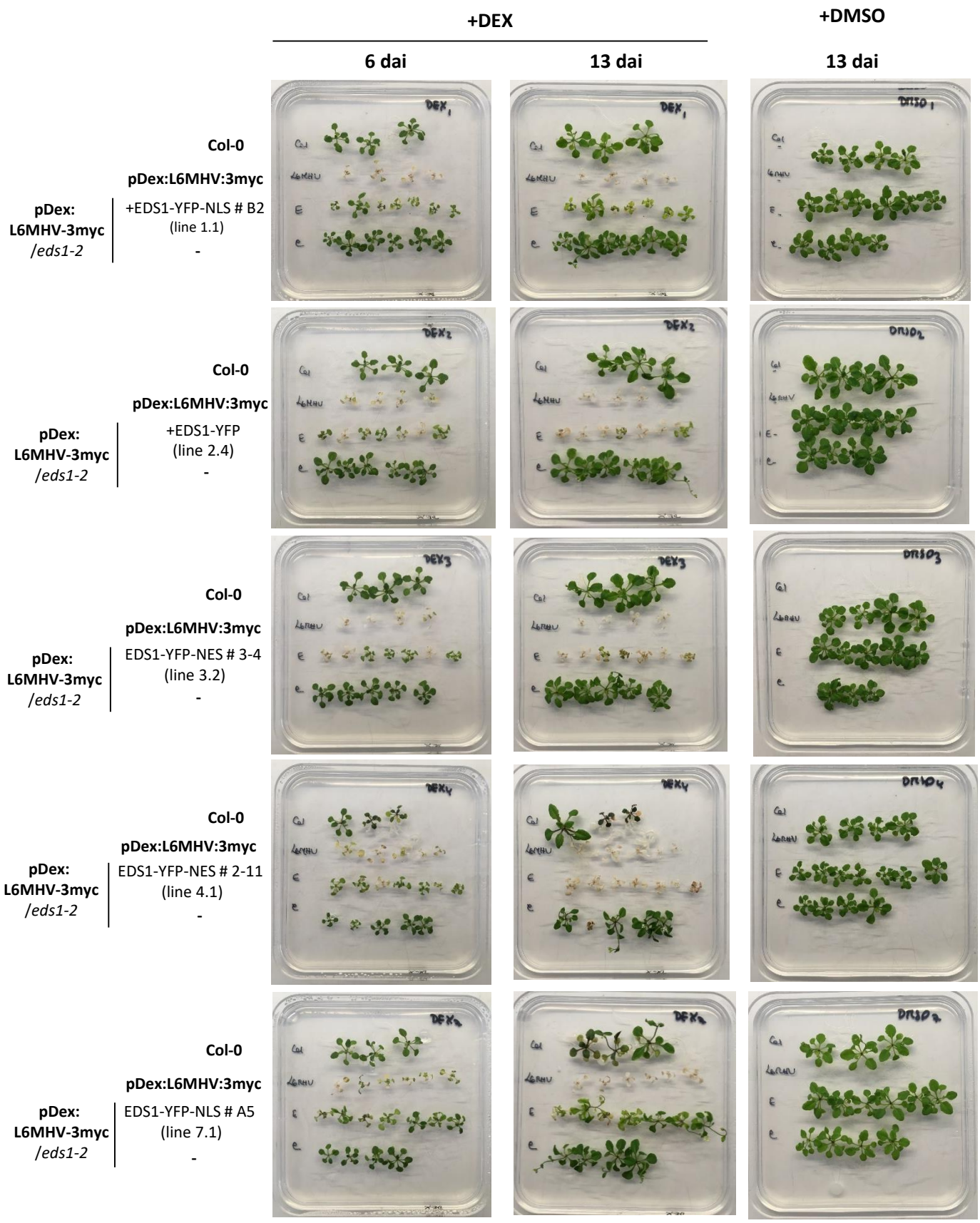

Figure S10: Phenotype of transgenic Arabidopsis seedlings from crosses of pDex:L6MHV-3myc/*eds1-2* line with independent mislocalized EDS1 variants lines. F3 individuals (12 day-old seedlings) from each cross (pDex:L6MHV-3myc x *eds1-2) x* pEDS1:EDS1-YFP mislocalized variants (pEDS1:EDS1-YFP-NLS (#B2), pEDS1:EDS1-YFP-NLS (#A5), pEDS1:EDS1-YFP-NES (#2-11), pEDS1:EDS1-YFP-NES (#3-4), pEDS1:EDS1-YFP-nls (#B5), pEDS1:EDS1-YFP-nes (#1-2)) were PCR screened to verify the presence or absence (-) of EDS1-YFP variant transgene and transferred to 10µM Dex-containing media. Photos were taken at six (6 dai) and thirteen (13 dai) days after transfer on Dex inducing media (DEX), and at 13 dai on non-inducing media (DMSO). On Dex-inducing media, transgenic pDex:L6MHV-3myc and wild-type Col-0 seedlings were used as positive and negative controls, respectively. On non-inducing media wild-type Col-0 seedlings were used as controls.

Figure S11: Subcellular localization of EDS1-YFP variants in Dex-inducible transgenic Arabidopsis seedlings (10 day-old) expressing pDex:L6MHV in *eds1-2* mutant background complemented with mislocalized EDS1-YFP variants. F3 individuals from each crosses (pDex:L6MHV x *eds1-2) x* pEDS1:EDS1-YFP mislocalized variants were PCR screened for the presence of EDS1-YFP variant (and transferred to inducing (Dex)-containing MS media. The roots of at least two seedlings were analysed by confocal microscopy. Images were taken 24h after Dex induction. Left: Yellow Fluorescence images, right: Overlay of brightfield and yellow fluorescence images. White scale represents 50µm.

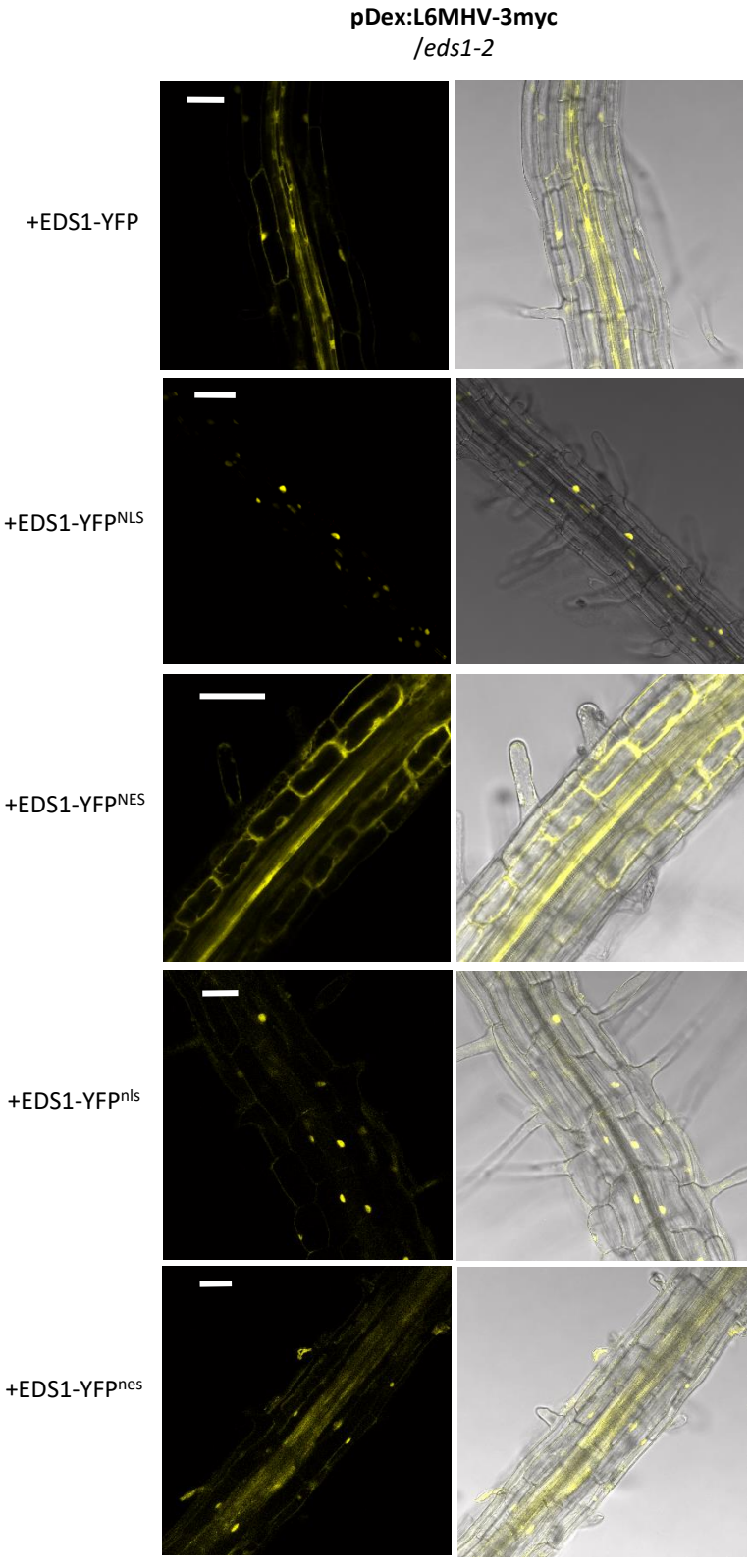

Figure S12: Phenotype of independent transgenic Arabidopsis seedlings expressing Dexamethasone (Dex)-inducible RPS4 $^{1-235}$-FSBP.

F2 individuals (10-day old) were transferred to non-inducing (DMSO) or 10µM Dex-containing media (DEX). Photos were taken 8 days after transfer.

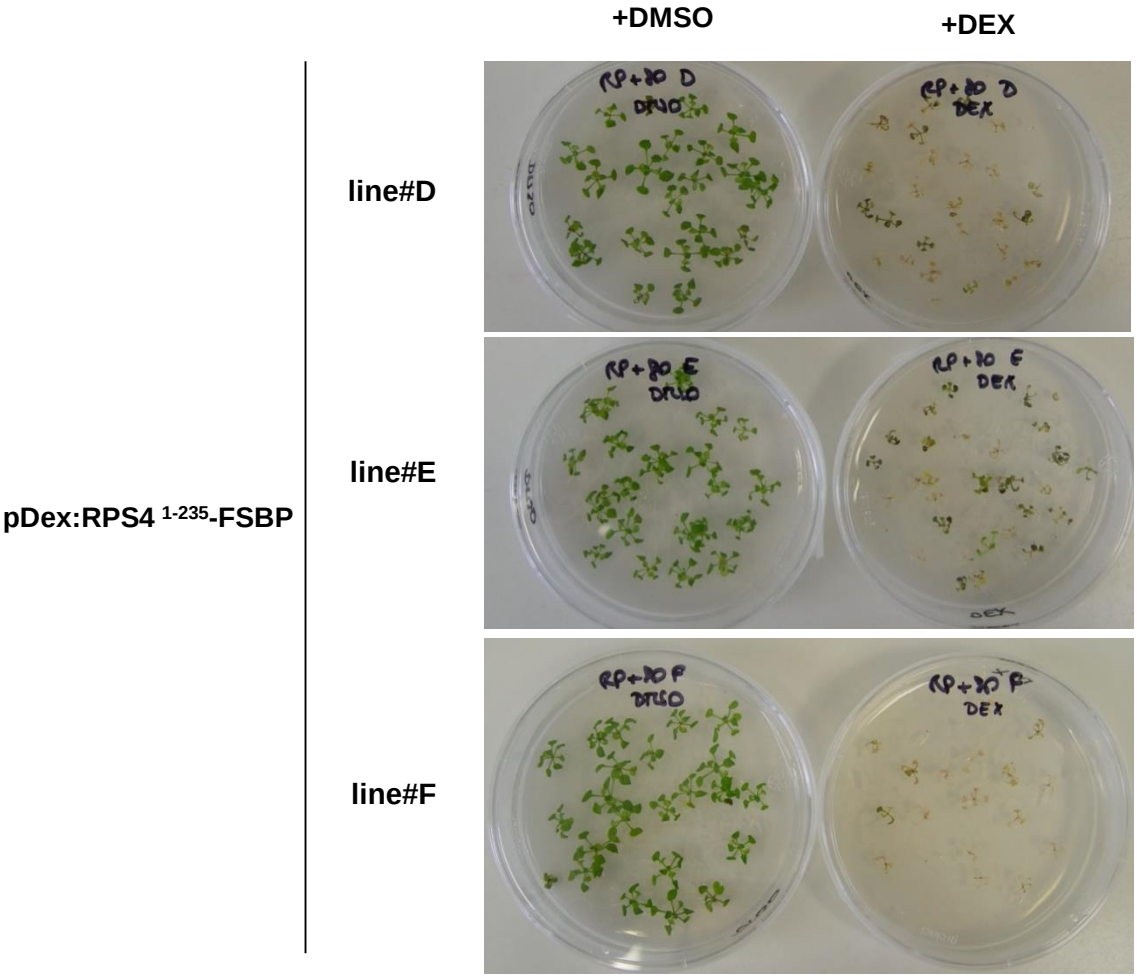

Figure S13: Phenotype of transgenic Arabidopsis seedlings expressing pDex:RPS4 $^{1-235}$ on a non-inducing media.

F3 individuals of Arabidopsis seedlings (10 day-old) expressing Dexamethasone (Dex)-inducible RPS4 $^{1-235}$ in wild-type Col-0 or in *eds1-2* mutant background complemented with mislocalized EDS1-YFP variants (pDex: RPS4 $^{1-235}$ –FSBP x *eds1-2) x* pEDS1:EDS1-YFP mislocalized variants. Each individuals were PCR screened to verify the presence or absence of EDS1-YFP variant transgene and transferred to non-inducing (DMSO containing) MS media. Photos were taken on the day plants were transferred (t0), four (3dai) and eight (6dai) days after transfer (dai: days after induction). This assay was performed two times with similar results.

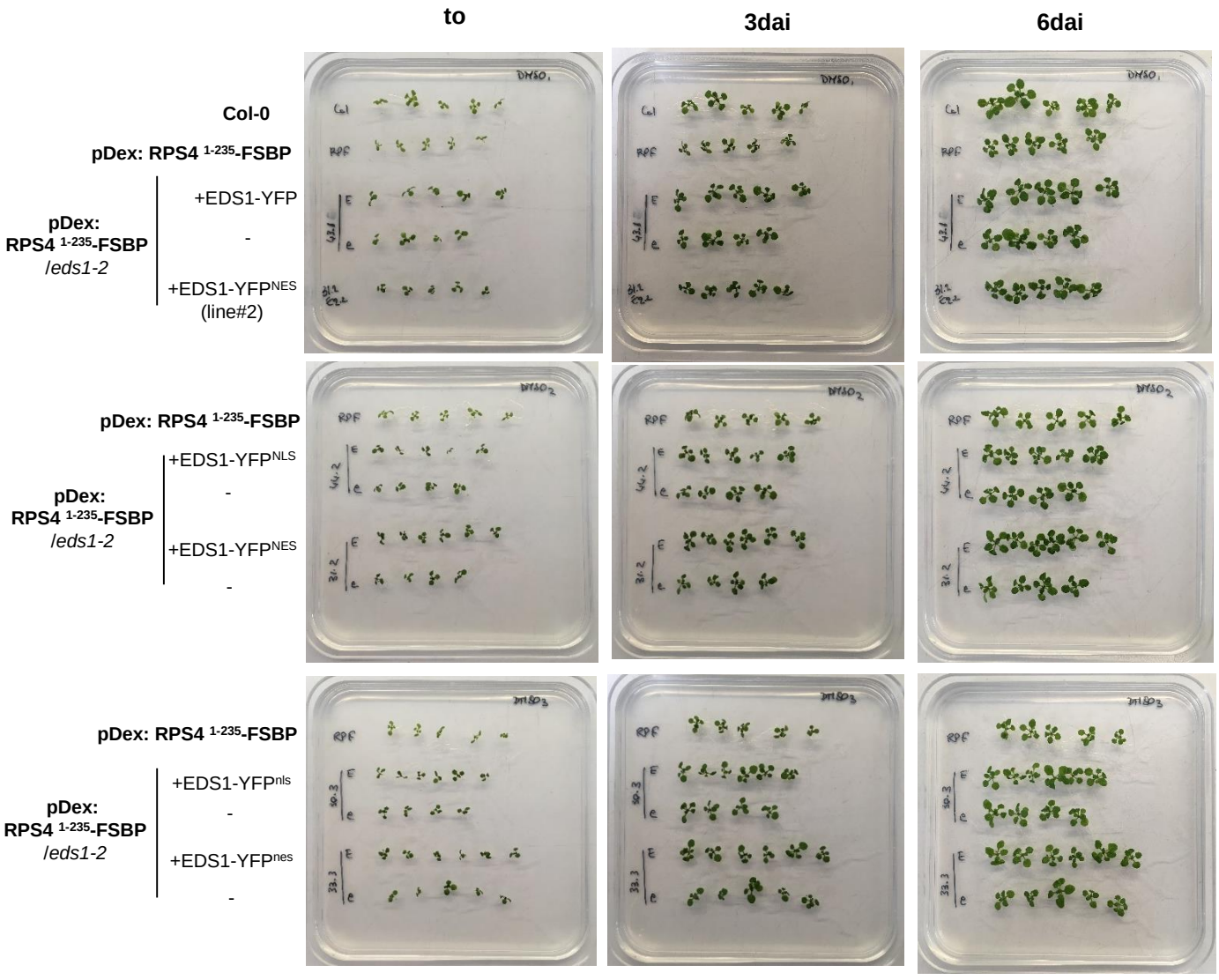

Figure S14: Phenotype of transgenic Arabidopsis seedlings from crosses of pDex: RPS4 $^{1-235}$-FSBP */eds1-2* line #8.1 with independent mislocalized EDS1 variants lines. F2 individuals (12 day-old seedlings) from each cross (pDex: (L6MHV-3myc x *eds1-2) x* pEDS1:EDS1-YFP mislocalized variants (pEDS1:EDS1-YFP-NLS (#B2), pEDS1:EDS1-YFP-NLS (#A5), pEDS1:EDS1-YFP-NES (#2-11), pEDS1:EDS1-YFP-NES (#3-4), pEDS1:EDS1-YFP-nls (#B5)), were PCR screened to verify the presence or absence (-) of EDS1-YFP variant transgene and transferred to 10µM Dex-containing media. Photos were taken at six days after transfer on Dex inducing media (DEX), or non-inducing media (DMSO). Wild-type Col-0 seedlings were used as negative controls.

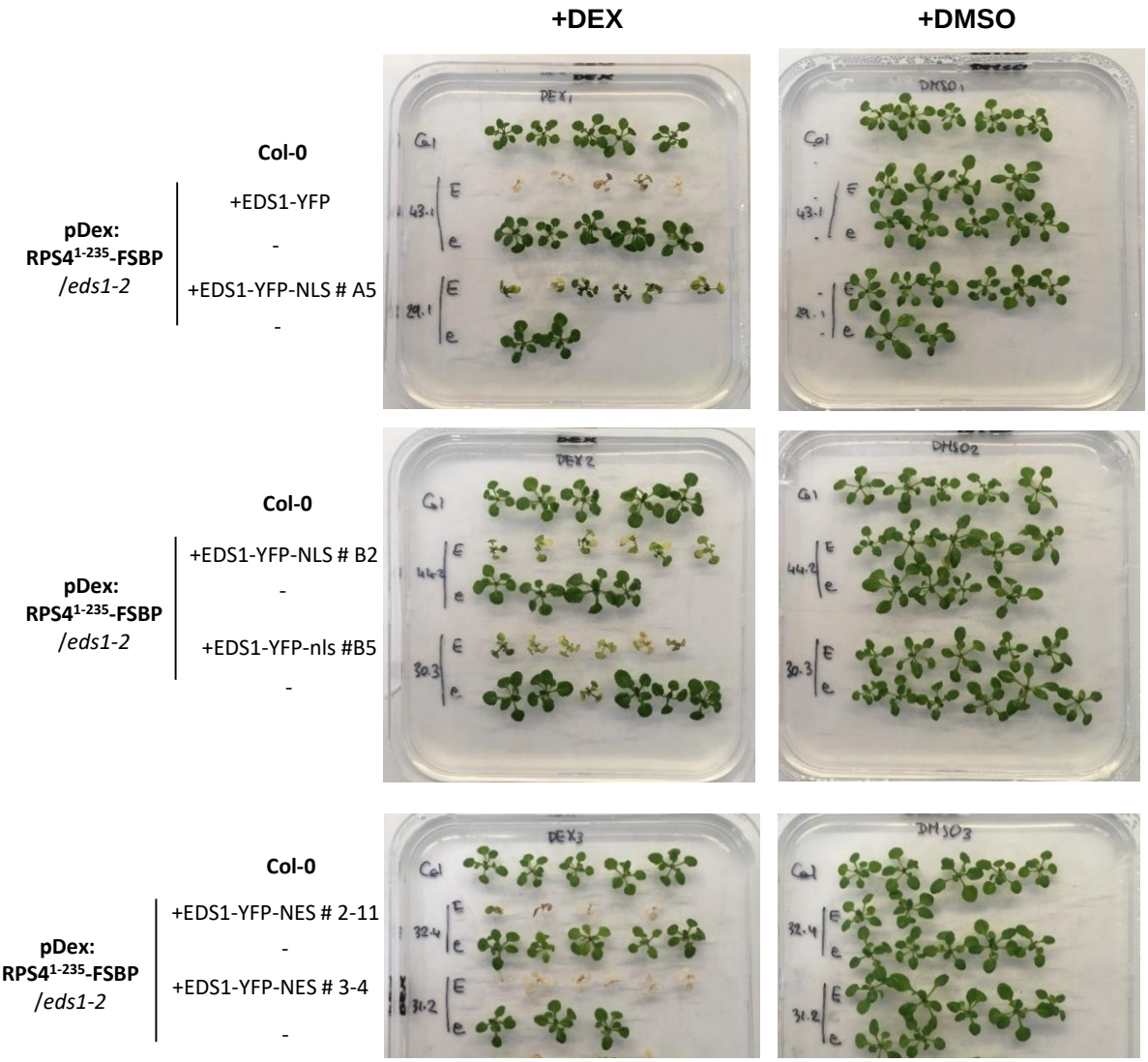

Figure S15: Subcellular localization of EDS1-YFP variants in Dex-inducible transgenic Arabidopsis seedlings (10 day-old) expressing pDex:RPS4 $^{1-235}$ in *eds1-2* mutant background complemented with mislocalized EDS1-YFP variants. F3 individuals from each crosses (pDex: RPS4 $^{1-235}$-FSBP x *eds1-2) x* pEDS1:EDS1-YFP mislocalized variants were PCR screened for the presence of EDS1-YFP variant (and transferred to inducing (Dex)-containing MS media. The roots of at least two seedlings were analysed by confocal microscopy. Images were taken 24h after Dex induction. Left: Fluorescence images, right: Overlay of brightfield and yellow fluorescence images. White scale represents 40µm.

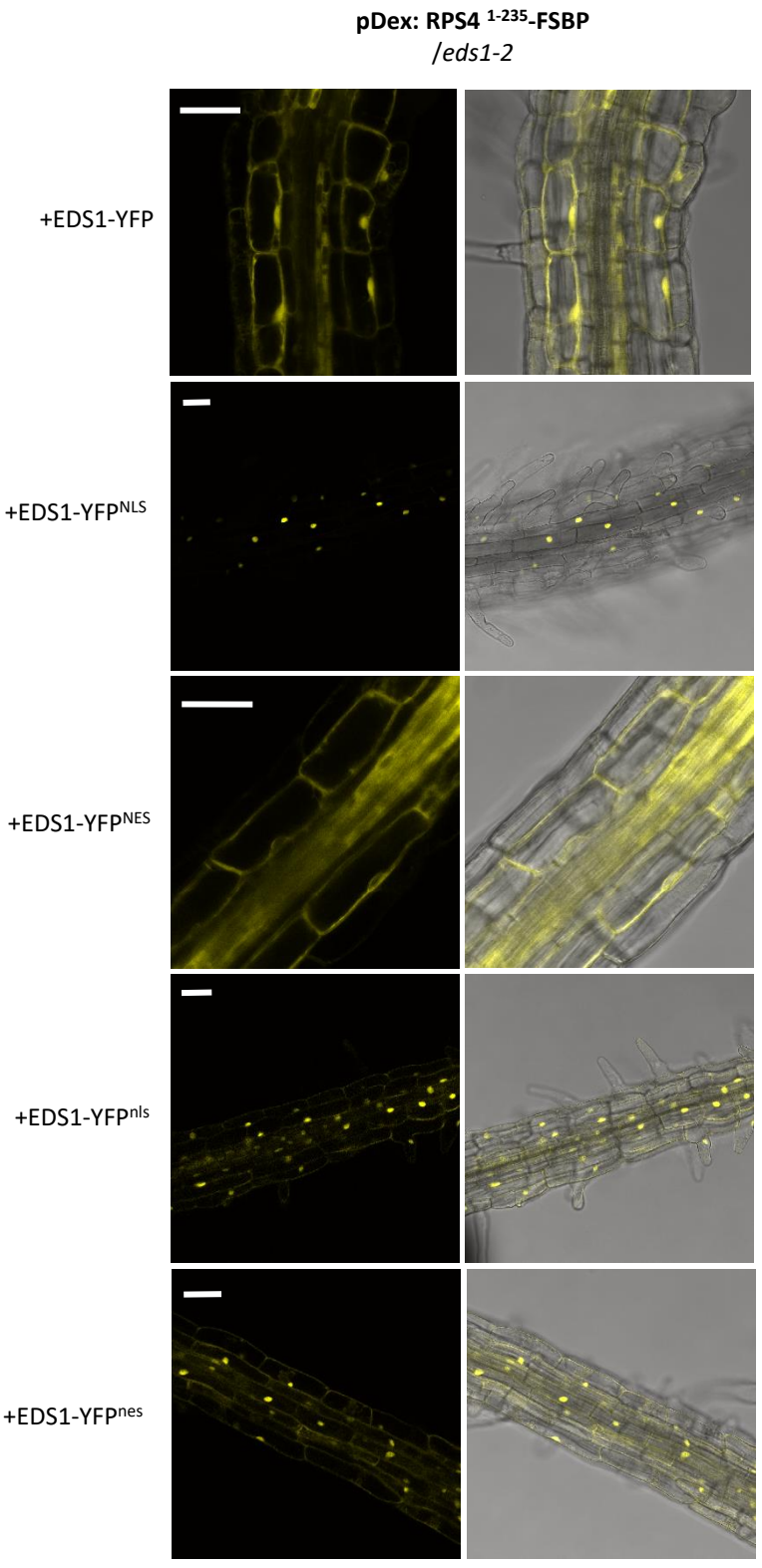

Figure S16: TIR signaling subcellular localization requirement model.
TIR domain (purple ovals) self-association leads to the production of TIR-catalysed signaling molecules (orange star), which is sensed by EDS1 family heterodimer (EDS1/PAD4 or EDS1/SAG101), which shuffle between the cytosolic and nuclear compartments. In turn, EDS1 heterodimer activation promotes interaction with RNL-type helper NLRs to activate transcriptionnal reprogramming in the nucleus and cell death in the cytosol via the formation of Ca^{2+} permeable channels at the plasma membrane (RNL resistosome). How Ca^{2+} signals is perceived and transduced by the cell to trigger cell death and/or immune reprogramming remains unknown.
Golgi-membrane anchored L6 can only trigger signaling from the cytosolic compartment while nucleocytosolic RPS4 and SNC1 TIRs can activate signaling from both cytosolic and nuclear compartments. Both type of TIRs can activate cell death and autoimmune responses when EDS1 is restricted to the cystosol but can activate immune responses but not cell death when EDS1 is sequestered in the nucleus.
Protein-protein interaction between EDS1 heterodimer and RNLs is represented as black double sensed arrows.
EDS1 is depicted as filled blue half-circle and SAG101/PAD4 partner as clear blue half-circle. RNLs resistosome CC domains are depicted as green cylinders.